

Observational estimates of the initial power spectrum at small scale from Lyman- α absorbers

M. Demiański^{1,2,3} and A. Doroshkevich^{3,4}

ABSTRACT

We present a new method of measuring the power spectrum of initial perturbations to an unprecedentedly small scale of $\sim 10h^{-1}$ kpc. We apply this method to a sample of 4500 Ly- α absorbers and recover the cold dark matter (CDM) like power spectrum at scales $\geq 300h^{-1}$ kpc with a precision of $\sim 10\%$. However at scales $\sim 10 - 300h^{-1}$ kpc the measured and CDM-like spectra are noticeably different. This result suggests a complex inflation with generation of excess power at small scales. The magnitude and reliability of these deviations depend upon the possible incompleteness of our sample and poorly understood process of formation of weak absorbers. Confirmation of the CDM-like shape of the initial power spectrum or detection of its distortions at small scales are equally important for widely discussed problems of physics of the early Universe, galaxy formation, and reheating of the Universe.

We use the Zel'dovich theory of gravitational instability to derive statistical description of the properties of observed structure. Our method links the observed mass function of absorbers with the correlation function of the initial velocity field and therefore it avoids the Nyquist restrictions limiting the investigations based on the smoothed flux or density fields. This approach is in general consistent with numerical simulations of the process of structure formation, describes reasonably well the Large Scale Structure observed in the galaxy distribution at small redshifts and emphasizes the generic similarity of galaxies and absorbers.

The physical model of absorbers adopted here asserts that they are formed in the course of both linear and nonlinear adiabatic or shock compression of dark matter (DM) and gaseous matter. It allows us to link the column density and overdensity of DM and gaseous components with observed characteristics of absorbers such as the column density of neutral hydrogen, redshifts and Doppler parameter. At scales $\geq 1h^{-1}$ Mpc all characteristics of the DM component and, in particular, their redshift distribution are found to be consistent with theoretical expectations for Gaussian initial perturbations with a CDM-like power spectrum.

Subject headings: Cosmology: observations – large scale structure – quasars: absorption lines

¹Institute of Theoretical Physics, University of Warsaw, 00-681 Warsaw, Poland.

²Department of Astronomy, Williams College, Williamstown, MA 01267, USA

³Theoretical Astrophysics Center, Juliane Maries Vej 30, DK-2100, Copenhagen, Denmark.

⁴Keldysh Institute of Applied Math. Russian Academy of Sciences, 125047, Moscow, Russia

1. Introduction

One of the most important problems of modern cosmology is to determine the power spectrum of primordial perturbations. This problem is closely connected with physics of the early Universe, properties of the inflation process, reionization of the Universe at moderate redshifts and formation of the Large Scale Structure (LSS) observed in deep galaxy surveys among others.

Presently various observational approaches are used to measure the power spectrum of the initial density perturbations. The amplitude and the shape of initial power spectrum on scales $\geq 10h^{-1}\text{Mpc}$ are approximately established by investigations of the relic radiation (Spergel et al. 2003) and the structure of the Universe at $z \ll 1$ detected in large redshift surveys (Percival et al. 2001; Peacock et al. 2001; Efstathiou et al. 2001; Tegmark, Hamilton & Xu 2002; Verde et al. 2002) and weak lensing data (see, e.g., Hoekstra, Yee & Gladders 2002). The shape of the initial power spectrum on scales $10h^{-1}\text{Mpc} - 1h^{-1}\text{Mpc}$ can be tested at high redshifts where it is not yet strongly distorted by nonlinear evolution (Croft et al. 1998, 2002; Nusser & Haehnelt 2000; Gnedin & Hamilton 2002). Recent results on reconstruction of the initial power spectrum are summarized and discussed in Tegmark and Zaldarriaga (2002), Wang et al. (2002) and Peiris et al. (2003).

Analysis of the observed absorption spectra of high redshift quasars seems to be the most promising method of recovering the power spectrum of initial perturbations at small scale. Indeed, the absorption lines trace the small scale hydrogen distribution along the line of sight at redshifts $z \geq 2$ when matter is not yet strongly clustered. The available Keck and VLT high resolution observations of the Lyman- α forest provide a sufficiently rich database which can be analyzed with the help of statistical methods.

The composition and spatial distribution of the observed absorbers is complicated and at low redshifts a significant number of stronger Ly- α lines and metal systems is associated with galaxies (Bergeron et al. 1992; Lanzetta et al. 1995; Tytler 1995; Le Brune et al. 1996). However as was recently shown by Penton, Stock and Shull (2002), even at small redshifts some absorbers are associated with galaxy filaments while others are

found within galaxy voids.

These results suggest that the population of weaker absorbers dominating at higher redshifts can be associated both with the periphery of rare high density objects and with weaker DM pancakes formed by the non luminous baryonic and DM components in extended low density regions. They suggest that the Ly- α forest can be considered as a low mass component of the generic LSS which is seen in simulated and observed spatial matter distribution. In turn, the relatively homogeneous spatial distribution of absorbers implies a more homogeneous spatial distribution of both DM and baryonic matter as compared with the observed distribution of the luminous matter.

Essential progress in understanding the process of formation and evolution of LSS has recently been achieved through numerous high resolution simulations which show that this process is mainly driven by the power spectrum of initial perturbations. These results were used in Demiański & Doroshkevich (1999, 2002; hereafter DD99 & DD02) to consider the properties of the LSS in the context of the nonlinear theory of gravitational instability (Zel'dovich 1970; Shandarin & Zel'dovich 1988). The statistical description of the process of structure formation and evolution developed in DD99 & DD02 links the directly measured characteristics of the structure such as the mass function of DM pancakes and walls, with the initial power spectrum.

This approach generalizes the Press-Schechter formalism (Press & Schechter 1974; Peacock & Heavens 1990; Bond et al. 1991; Loeb & Barkana 2001) and describes the formation and evolution of all DM structure elements for the CDM or WDM initial power spectra without any smoothing or filtering procedures. The evolution of structure proceeds through random formation and merging of Zel'dovich pancakes, their transverse expansion and/or compression and subsequent transformation into high density clouds and filaments. Later on the hierarchical merging of pancakes, filaments and clouds forms rich galaxy walls observed at small redshifts. The main stages of this evolution are driven by the initial power spectrum.

As is well known, the Zel'dovich approach correctly describes both the linear and mildly nonlinear stages of the structure formation but it cannot describe the processes of violent relaxation and the

final stage of formation of gravitationally bound object. In spite of this, the statistical approach proposed in DD99 and DD02 nicely describes the main properties of observed and simulated LSS (Demiański et al. 2000; Doroshkevich, Tucker & Allam 2002). In particular, comparison of characteristics of simulated DM distribution and observed galaxy walls with theoretical expectations allows one to restore the amplitude and shape of initial power spectrum at appropriate scales.

Early application of the *truncated* Zel'dovich approximation for the description of the Ly- α forest was critically mentioned in Bond and Wadley (1997) but their criticism was not supported by more detailed investigation. In contrast, the Zel'dovich approach has been considered as very promising by Hui, Gnedin and Zhang (1997) and Hui (1997) who applied it to describe the Doppler parameter and neutral hydrogen column density. However, these characteristics depend upon random variations of the gas entropy and, so, their theoretical description is quite problematic.

The statistical approach proposed in DD02 was used in Demiański, Doroshkevich & Turchaninov (2003, hereafter Paper I) to describe properties of absorbers observed in 14 high resolution spectra. This approach deals with DM characteristics of absorbers. Evolution of DM component of absorbers is driven mainly by the gravitational interaction and it can be approximately described theoretically. However in this approach the DM characteristics of absorbers are expressed through the observed ones what in turn requires a physical model of absorbers.

Such model, introduced in Paper I, allows one to find a physically motivated combination of observed characteristics of absorbers which are consistent with theoretically expected ones for the DM pancakes. These results allows us to interpret this combination as actual characteristic of DM component of absorbers and confirm the self consistency of the proposed physical model of absorbers. They show also that the statistical approach proposed in DD99 and DD02 provides a reasonable description at least for so defined DM characteristics of absorbers. However, we cannot theoretically describe more complex evolution of the gaseous component of absorbers, their Doppler parameters and column density of neutral hydrogen.

Following Paper I, also in this paper we consider that absorbers are dominated by long-lived gravitationally bound and partially relaxed objects formed in the course of both adiabatic and shock compression. Observations of galaxies and quasars at $z \geq 3$ and the reheating of the Universe at redshifts $z \geq 6$ demonstrate the importance of nonlinear processes at such redshifts and support our approach. Numerous simulations (see, e.g. Frenk 2002) confirm the formation of high density DM filaments and sheets at similar redshifts ($z \geq 2$). The typical size and mass of such objects progressively increase with time and now richer objects are seen as the LSS in the galaxy distribution. In this paper we assume that absorbers at high z trace the DM structure which is qualitatively similar to the rescaled one observed at small redshifts. However, for less massive pancakes properties of the baryonic and DM components differ due to the influence of gaseous pressure.

Here we use this approach to recover the initial power spectrum to unprecedentedly small scales. In contrast with previous investigations (Croft et al. 1998, 2002; Nusser & Haehnelt 2000) we analyse the DM mass function of absorbers rather than the flux or smoothed density field. This means that our results are not restricted by the standard factors such as the Nyquist limit, the impact of nonlinear processes, the unknown matter distribution between absorbers or their peculiar velocities. The reliability and precision of our method have been tested on the simulated DM and observed galaxy surveys (Demiański et al. 2000; Doroshkevich, Tucker & Allam 2002).

At scales $\geq 1h^{-1}\text{Mpc}$ our estimates of the initial power spectrum are consistent with the CDM-like one with precision $\sim 10\%$. However, we found some evidence that at scales $\leq 1h^{-1}\text{Mpc}$ the initial power spectrum differs from the CDM-like one suggesting a complex inflation with generation of excess power at small scales. Such excess power accelerates the process of galaxy formation at high redshifts and shifts the epoch of reheating of the Universe, which perhaps began at $z = 20 \pm 10$ (Kogut et al. 2003) and continued up to $z \approx 6$ (Djorgovski et al 2001; Fan et al. 2001, 2003). More detailed discussion of the process of reionization can be found in Ciardi, Ferrara & White (2003) and Cen (2003).

At present we have only limited information about the properties of the background gas and UV radiation (Scott et al. 2000; Schaye et al. 2000; McDonald & Miralda-Escude 2001; McDonald et al. 2000, 2001; Theuns et al. 2002 a, b) and therefor some numerical factors in our model remain undetermined. This means that our approach should be tested on representative numerical simulations which more accurately follow the process of formation and disruption of pancakes and filaments and provide a unified picture of the process of absorbers formation and evolution (see, e.g., Weinberg et al. 1998; Zhang et al. 1998; Davé et al. 1999; Theuns et al. 1999). However, as was shown by Meiksin, Bryan & Machacek (2001), available simulations reproduce quite well the characteristics of the flux but cannot restore other observed characteristics of the forest. This means that first of all numerical simulations should be improved (see Sec. 9.4).

This paper is organized as follows. In Secs. 2 & 3 a short theoretical description of structure formation and the physical model of absorbers are presented. In Sec. 4 the observational databases used in our analysis and redshift evolution of the observed absorber characteristics are described. Results of statistical analysis are given in Secs. 5 and 6 and their reliability and precision are discussed in Sec. 7. In Sec. 8 we link the measured correlation function with the power spectrum. Discussion and conclusions can be found in Sec. 9.

2. Initial power spectrum and characteristics of DM pancakes

2.1. Basic cosmological model

In this paper we consider the spatially flat Λ CDM model of the Universe with the Hubble parameter and mean matter density given by:

$$H^2(z) = H_0^2 \Omega_m (1+z)^3 [1 + \Omega_\Lambda / \Omega_m (1+z)^{-3}], \quad (1)$$

$$\langle \rho_m(z) \rangle = \frac{3H_0^2}{8\pi G} \Omega_m (1+z)^3, \quad H_0 = 100h \text{ km/sMpc}.$$

Here $\Omega_m = 0.3$ & $\Omega_\Lambda = 0.7$ are dimensionless matter density and the cosmological constant (dark energy), and $h = 0.7$ is the dimensionless Hubble constant.

We assume that the baryonic background is characterized by the following parameters

$$\langle n_b(z) \rangle = 2.4 \cdot 10^{-7} \text{ cm}^{-3} (1+z)^3 (\Omega_b h^2 / 0.02), \quad (2)$$

$$T_{bg} \approx 1.6 \cdot 10^4 K, \quad b_{bg} = \sqrt{\frac{2k_B T_{bg}}{m_H}} \approx 16 \text{ km/s}.$$

Here Ω_b , T_{bg} & b_{bg} are the dimensionless density, temperature and Doppler parameter of the baryonic component, k_B & m_H are the Boltzmann constant and the mass of hydrogen atom.

2.2. The initial power spectrum

As a reference power spectrum of initial perturbations we take the standard CDM-like spectrum with the Harrison – Zel’dovich asymptotic,

$$P(k) = \frac{A^2 k}{4\pi k_0^4} T^2(k/k_0) D_W(k) D_J(k), \quad k_0 = \frac{\Omega_m h^2}{\text{Mpc}}, \quad (3)$$

where A is the dimensionless amplitude of perturbations, k is the comoving wave number. The transfer function, $T(k)$, and the damping factor $D_W(k)$ describing the free streaming of DM particles were given in Bardeen et al. (1986). The factor $D_J(k)$ describes the dumping of small scale baryonic perturbations (Jeans scale) and the bias between perturbations of DM and baryonic components (see, e.g., Mattarese & Mohayaee 2002). However, characteristics of the DM structure elements are defined by (3) with $D_J(k) \equiv 1$.

For WDM particles the dimensionless damping scale, R_f , and the damping factor, D_W , are

$$R_f = \frac{1}{5} \left(\frac{\Omega_m h^2 \text{ keV}}{M_{DM}} \right)^{4/3}, \quad D_W = \exp[-\eta R_f - (\eta R_f)^2],$$

where $\eta = k/k_0$ and M_{DM} is the mass of WDM particles (Bardeen et al. 1986). The Jeans wave number, k_J , and the damping factor, D_J , can be taken as

$$k_J^{-1} \approx 0.7 b_{bg} (1+z) H^{-1}(z), \quad D_J \approx (1 + \eta_J^2 \eta^2)^{-1},$$

$$\eta_J = k_0/k_J \approx 2 \cdot 10^{-2} \sqrt{\frac{\Omega_m h^2}{0.13}} \sqrt{\frac{4}{1+z}} \frac{b_{bg}}{16 \text{ km/s}}.$$

Here as a reference we use the values of the background parameters specified by (2).

The amplitude of initial perturbations, A , is now measured reasonably well with different methods. It is simply linked with σ_8 , the variance of

the mass within a randomly placed sphere of radius $8h^{-1}\text{Mpc}$,

$$\sigma_8^2 = 9A^2 \int_0^\infty d\eta \eta^3 T^2(\eta) \left(\frac{\sin \eta_8 - \eta_8 \cos \eta_8}{\eta_8^3} \right)^2, \quad (4)$$

where $\eta = k/k_0$ and $\eta_8 = 8\eta\Omega_m h$. Here we use the latest estimates (Spergel et al. 2003) for the model (1)

$$\sigma_8 \approx 0.055A \approx 0.9 \pm 0.1, \quad A \approx 16.4 \pm 1.82. \quad (5)$$

2.3. Coherent lengths and correlation functions of the initial perturbations

For the spectrum (3) the coherent lengths of velocity and density fields, l_v & l_ρ , are expressed through the spectral moments, m_{-2} & m_0 , as follows:

$$l_v = \frac{1}{k_0 \sqrt{m_{-2}}} = \frac{6.6}{\Omega_m h^2} \text{Mpc} \approx 33.8 h^{-1} \text{Mpc} \frac{0.13}{\Omega_m h^2}, \quad (6)$$

$$m_{-2} = \int_0^\infty d\eta \eta T^2(\eta) D_W(\eta) D_J(\eta) \approx 0.023, \quad l_\rho = q_0 l_v,$$

$$m_0 = \int_0^\infty d\eta \eta^3 T^2(\eta) D_W(\eta) D_J(\eta), \quad q_0 = 5 \frac{m_{-2}^2}{m_0}.$$

The analysis of the redshift distribution of Lyman- α clouds (Paper I) allowed us to estimate the moment m_0 that in turn restricts the expected Jeans scale and the mass of the dominant fraction of DM particles. These estimates

$$q_0 \approx (0.6 - 1.2) \cdot 10^{-2}, \quad \eta_J \approx 0.01 - 0.02, \quad (7)$$

$$M_{DM} \approx (1.5 - 5) \text{keV}, \quad R_f \approx (7.7 - 1.5) \cdot 10^{-3},$$

are close to those of Narayanan et al. (2000), $M_{DM} \geq 0.75$ keV, and Barkana, Haiman & Ostriker (2001), $M_{DM} \geq 1 - 1.25$ keV. However, as was discussed in Paper I, the Jeans damping, D_J , restricts abilities of this approach, and to test the small scale power spectrum we have to use characteristics of DM component of absorbers for which $D_J = 1$.

As was demonstrated in DD99 and DD02, main statistical characteristics of structure are expressed through the normalized longitudinal correlation function of the initial velocity field

$$\xi_v(q) = 3 \frac{\langle (\mathbf{q} \cdot \mathbf{v}(\tilde{\mathbf{q}}_1)) (\mathbf{q} \cdot \mathbf{v}(\tilde{\mathbf{q}}_2)) \rangle}{\sigma_v^2 q^2}, \quad \mathbf{q} = \frac{\tilde{\mathbf{q}}_1 - \tilde{\mathbf{q}}_2}{l_v}. \quad (8)$$

Here $\tilde{\mathbf{q}}_1$ & $\tilde{\mathbf{q}}_2$ are the unperturbed coordinates of two particles at $z = 0$, $q = |\mathbf{q}|$, and σ_v^2 is the velocity variance. This function is expressed through the power spectrum:

$$\xi_v = \frac{3}{m_{-2}} \int_0^\infty d\eta \eta^2 \cos x \int_\eta^\infty \frac{dy}{y^2} T^2(y) D_W(y) = \quad (9)$$

$$\frac{\sqrt{\pi/2}}{m_{-2}} \int_0^\infty \frac{d\eta}{\sqrt{x}} [J_{1/2}(x) - 2J_{5/2}(x)] \eta T^2(\eta) D_W,$$

where $x = q\eta$, $J_{1/2}(x)$ and $J_{5/2}(x)$ are Bessel functions. From (9) it follows that $\xi_v(0) = 1$ and $\int_0^\infty dq \xi(q) = 0$. For the CDM-like spectrum (3) and for the most interesting ranges $q_0 \leq 10^{-2}$, $0.5 \geq q \geq 10^{-3}$, the velocity correlation function can be fitted as follows:

$$\xi_v = \xi_{CDM} \approx 1 - \frac{q^2}{\sqrt{u_0(q)u_1(q)}} \frac{q_0 + 1.5u_0(q)}{q_0 + u_0(q)}. \quad (10)$$

$$u_0 = \sqrt{q^2 + q_0^2}, \quad u_1 = \sqrt{q^2 + 3 \cdot 10^{-4}}$$

Further on, we will use this function with $q_0 = 0.01$ as the reference one and will compare it with observational estimates of $\xi_v(q)$. This value of q_0 lies in the range of (7) and corresponds to the mass of WDM particles $M_{WDM} \approx 3$ keV (or the Jeans damping scale for $T_{bg} \approx 10^4 \text{K}$).

2.4. Characteristics of DM pancakes

We use the Zel'dovich approximation (Zel'dovich 1970; Shandarin & Zel'dovich 1989) to relate the characteristics of the initial density perturbations with the properties of observed pancakes. As was discussed in DD99, DD02 and Paper I, three quantitative characteristics of pancakes can be used for the comparison with observations. Two of them are the differential, N_q , and cumulative, W_q , distribution functions (PDFs) of the dimensionless DM surface density (or column density) of pancakes, q . The DM surface density is defined as the dimensionless unperturbed distance at redshift $z = 0$ between DM particles bounding the pancake (8). The third characteristic is the dimensionless mean number density of absorbers (Lyman- α clouds), $n_{abs}(q_{thr}, z)$. All these characteristics depend upon the distribution function of the initial density perturbations which can be taken as Gaussian (Komatsu et al. 2003), upon the correlation function of the initial velocity field,

$\xi_v(q)$, and the survival probability of pancakes, $W_s(q)$, (DD99, DD02). The survival probability of clouds was introduced by Peacock & Heavens (1990) and Bond et al. (1991) to describe, in the framework of Press–Schechter approach, the difference between the fraction of matter accumulated by clouds and their mass function.

As was shown in DD99 and DD02, both PDFs and the survival probability depend upon the self similar variable

$$\zeta = \frac{q^2}{4\tau^2(z)[1 - \xi_v(q)]}, \quad (11)$$

where the ‘time’ $\tau(z)$ describes the growth of perturbations due to the gravitational instability. For the Λ CDM cosmological model (1), and for $z \geq 2$ we have

$$\tau(z) \approx \tau_0 \left(\frac{1 + 1.2\Omega_m}{2.2\Omega_m} \right)^{1/3} \frac{1}{1+z} \approx \frac{1.27\tau_0}{1+z}, \quad (12)$$

$$\tau_0 = Am_{-2}/\sqrt{3} \approx 0.22 \pm 0.02, \quad (13)$$

where A was introduced in (3) and (5).

For the Gaussian initial perturbations the matter fraction accumulated by structure elements is proportional to $\text{erfc}(\zeta) = 1 - \text{erf}(\zeta)$, where $\text{erf}(\zeta)$ is the standard error function. Following Peacock & Heavens (1990) and Bond et al. (1991), we assume that the mass function of the DM column density of pancakes and the matter fraction accumulated by pancakes differ by the survival probability, $W_s(\zeta)$. For low mass pancakes $W_s \ll 1$, what reflects stronger correlation of small scale perturbations, and $W_s \rightarrow 1$ with increasing mass of pancakes.

Analysis of simulated and observed structure at small redshifts (DD99; Doroshkevich, Tucker & Allam 2002) shows that for richer pancakes and galaxy walls the cumulative and differential PDFs, W_q & N_q , for the DM column density can be written as follows:

$$W_q(\zeta) = \text{erf}^2(\sqrt{\zeta}), \quad N_q = \frac{2}{\sqrt{\pi}} e^{-\zeta} \frac{\text{erf}(\sqrt{\zeta})}{\sqrt{\zeta}} \frac{d\zeta}{dq}, \quad (14)$$

with the survival probability $W_s = \text{erf}(\sqrt{\zeta})$. However, other expressions for the survival probability can be also used and, for comparison, here we consider the model with $W_s = \text{erf}^2(\sqrt{\zeta})$ and

$$W_q(\zeta) = \text{erf}^3(\sqrt{\zeta}), \quad N_q = \frac{3}{\sqrt{\pi}} e^{-\zeta} \frac{\text{erf}^2(\sqrt{\zeta})}{\sqrt{\zeta}} \frac{d\zeta}{dq}. \quad (15)$$

This problem is further discussed in Sec. 7.

The dimensionless mean number density of absorbers, $n_{abs}(q_{thr}, z)$, with the above assumptions is given by:

$$n_{abs} \approx \frac{c}{H_0 l_v} \frac{\text{erfc}(\zeta_{thr})(1+z)^2}{\langle q(\zeta_{thr}) \rangle}. \quad (16)$$

Here $\text{erfc}(\zeta_{thr})$ describes the progressive matter concentration within pancakes with $\zeta \geq \zeta_{thr} = \zeta(z, q_{thr})$ and q_{thr} is the minimal (threshold) DM column density of pancakes in the sample under consideration (DD02, Paper I). For $W_s = \text{erf}(\sqrt{\zeta})$ and for $q_{thr} \gg q_0$, we get

$$\langle q(\zeta_{thr}) \rangle = 4\tau^2 \left[1 + \frac{4\sqrt{\pi\zeta_{thr}}\text{erf}(\sqrt{\zeta_{thr}}) + 2\exp(-\zeta_{thr})}{\pi \exp(\zeta_{thr})[1 - \text{erf}^2(\sqrt{\zeta_{thr}})]} \right]$$

where $\zeta_{thr}(z) = q_{thr}/6\tau^2(z)$. Similar relations can be also written for other survival probabilities.

For pancakes with small $q_{thr} \sim q_0$ the redshift variations of the mean number density $n_{abs}(z, q_{thr})$ are described by the expression

$$n_{abs} \approx \frac{c\sqrt{3}}{4\pi H_0 l_v} \frac{(1+z)^2 \exp(-\zeta_{thr})}{\sqrt{q_0[1 - \xi_v(q_{thr})]}} W_s(\zeta_{thr}), \quad (17)$$

with q_0 as given by (7) (DD02, Paper I). This approach considers only gaseous pancakes and, as was noted in Sec. 2.3, its sensitivity to the small scale perturbations is restricted by the Jeans damping.

2.5. Reconstruction of the initial power spectrum

Using the measured redshift, z , and DM column density of absorbers, q , we determine the cumulative PDF of absorbers $W_{obs}[> q/\tau(z)]$ and, for each $q/\tau(z)$, we compute $\langle q \rangle$ and $\sigma_q^2 = \langle q^2 \rangle - \langle q \rangle^2$. For a chosen $W_q(\zeta)$, we solve numerically the equation

$$W_{obs}[> q/\tau(z)] = W_q(\zeta), \quad (18)$$

with respect to $\zeta(q, \tau)$ and, thus, we obtain the function

$$\xi_v(q) = 1 - \frac{q^2}{4\tau^2\zeta}. \quad (19)$$

The observed functions $N_q(\zeta)$ and $n_{abs}(z)$ can be compared with corresponding expectations (14) – (16) for the correlation function $\xi_v(q)$ (19). This $\xi_v(q)$ can be also compared with the reference function $\xi_{CDM}(q)$ (10).

3. Determination of the DM column density

To connect the main observational characteristics of the Lyman- α absorption lines, namely, the redshift, z_{abs} , the column density of neutral hydrogen, N_{HI} , and the Doppler parameter, b , with the dimensionless DM column density, q , we use the improved model of absorbers discussed in Paper I. Here we only briefly summarize the main assumptions and relations. Detailed discussion of the model can be found in Paper I.

3.1. Physical model of absorbers.

Following Paper I we assume that:

1. The DM distribution forms an interconnected structure of sheets (Zel'dovich pancakes) and filaments. The baryonic component follows the DM distribution and therefore the main parameters of absorbers are approximately described by the Zel'dovich theory of gravitational instability (Sec. 2; DD99; DD02).
2. The majority of DM pancakes are partly relaxed, and long-lived, but the observed properties of absorbers vary with time due to the successive merging, transversal compression and/or expansion and disruption of DM pancakes.
3. Gas is trapped in the gravitational potential wells formed by the DM distribution. The gas temperature and the observed Doppler parameter, b , trace the depth of the DM potential wells. We consider the possible macroscopic motions within pancakes as subsonic and assume that they cannot essentially distort the measured Doppler parameter.
4. The gas is ionized by the UV background and for the majority of absorbers ionization equilibrium is assumed.
5. For a given temperature, the gas density within the potential wells is determined by the gas entropy created during the previous evolution. The gas entropy is changing, mainly, due to shock heating in the course of pancakes merging, bulk heating by the

UV background and local sources, and due to radiative cooling. Random variations of the intensity and spectrum of the UV background enhance random scatter of the observed properties of absorbers.

This model implies that the Ly- α clouds trace the LSS in the DM component which is qualitatively similar to the rescaled structure observed at $z \leq 1$ in the galaxy distribution. It links the characteristics of the DM structure and the observed absorption lines and, as was shown in Paper I, provides a reasonable self consistent description, at least, of richer absorbers. Our model considers discrete absorbers and, so, it essentially differs from the popular model of "fluctuating Gunn-Peterson approximation" discussed more thoroughly in Sec. 9.4.

Our approach cannot be applied to objects for which the gravitational potential and the gas temperature along the line of sight strongly depends on the matter distribution across this line. However, the anisotropic halos of filaments and clouds with moderate N_{HI} can be considered as 'pancake-like'.

Special attention require description of weaker absorbers with $b \leq b_{bg}$. This subpopulation contains "artificial" caustics (McGill 1990) and absorbers identified with slowly expanding underdense regions (Bi & Davidsen 1997; Zhang et al. 1998; Davé et al. 1999). Such absorbers produce a short lived noise, which is stronger at higher redshifts $z \geq 3$. However, such absorbers can also be formed within low temperature regions arising owing to spatial nonhomogeneities of the UV background and expansion rate. Strictly speaking our model does not include such absorbers because we assume that $b \geq b_{bg}$ for all absorbers formed due to compression of background matter and we suppose that b_{bg} is constant and it does not depend on the position or time. However, we can include absorbers with $b \leq b_{bg}$ into consideration assuming that they are adiabatically compressed but not bound gravitationally.

3.2. DM column density of absorbers

In this section we use the physical model discussed in Sec. 3.1 to introduce the basic relations between theoretical and observed characteristics of pancakes. The most important characteristics

of DM pancakes are presented (without proofs) as a basis for further analysis. More details are given in DD99, DD02, and Paper I.

The fundamental characteristic of DM pancakes is the dimensional, $\mu(z)$, or the dimensionless, q , DM surface density (the dimensionless DM column density) :

$$\mu(z) \approx \frac{\langle \rho_m(z) \rangle l_v q}{(1+z)}, \quad (20)$$

where the coherent length of the initial velocity field l_v was introduced in (6). As was discussed in Sec. 2.4, $l_v q$ is defined as the unperturbed distance at redshift $z = 0$ between DM particles bounding the pancake.

As was assumed in Sec. 3.1, we consider majority of absorbers as gravitationally bound and relaxed long lived DM pancakes. Their properties are slowly changing mainly owing to the process of merging and transverse expansion and compression. For such absorbers, the gas temperature, T_g , and the Doppler parameter, $b \propto \sqrt{T_g}$ (2) are closely linked with the gravitational potential of the DM pancake and we get:

$$\beta^2 = \frac{b^2}{b_{bg}^2} \approx 1 + \frac{4}{5} \frac{\pi G \mu^2 \Theta_\Phi}{b_{bg}^2 \langle \rho(z) \rangle \delta_m} = 1 + \delta_0 \frac{q^2}{\delta_m} (1+z), \quad (21)$$

$$\delta_0 = \frac{3}{10} \left(\frac{H_0 l_v}{b_{bg}} \right)^2 \Omega_m \Theta_\Phi \approx 4 \cdot 10^3 \frac{0.13}{\Omega_m h^2} \left(\frac{16 \text{ km/s}}{b_{bg}(z)} \right)^2 \Theta_\Phi.$$

Here δ_m is the mean overdensity of the DM pancake and the random factor $\Theta_\Phi \sim 1$ describes the nonhomogeneity of DM distribution across the pancake.

Under the condition of ionization equilibrium, for the column density of neutral hydrogen, we get

$$N_{HI} = \frac{2 \cdot 10^{16} \text{ cm}^{-2}}{\delta_0 G_{12}(z)} \delta_b q \beta^{-3/2} (1+z)^5 \quad (22)$$

$$= \frac{2 \cdot 10^{16} \text{ cm}^{-2}}{G_{12}(z)} \frac{q^3 (1+z)^6}{\beta^{7/2}} \frac{\beta^2}{\beta^2 - 1} \frac{\delta_b}{\delta_m},$$

$$G_{12} = \frac{\Gamma_{12}(z) \cos \theta}{\Theta_g(z)} \frac{1}{0.5} \left(\frac{\Omega_m h^2}{0.13} \frac{0.02}{\Omega_b h^2} \right)^2 \left(\frac{b_{bg}}{16 \text{ km/s}} \right)^{7/2} \quad (23)$$

where $\Gamma_{12} = \Gamma_\gamma / 10^{-12} \text{ s}^{-1}$, Γ_γ characterizes the rate of ionization of hydrogen by the UV background, δ_b is the overdensity of baryonic component, $\cos \theta$ describes a random orientation of the

absorber and the line of sight and the function $\Theta_g(z) \sim 1$ describes the action of several random and unknown factors (more details are given in Paper I).

The equations (21) and (22) relate three independent variables, namely, q , δ_b & δ_m . To find the DM column density, q , it is therefore necessary to use an additional relation which connects the basic properties of absorbers. In Paper I we assumed that $\beta \geq 1$, $\delta_m \approx \delta_b$. These assumptions are valid for richer absorbers formed due to strong shock compression when the essential growth of the entropy and temperature suppresses differences between the DM and baryonic components and so their distribution across the absorber is similar. For the DM column density of such absorbers we get

$$q^3 \approx \left(\frac{N_{HI}}{2 \cdot 10^{16} \text{ cm}^{-2}} \right) \frac{\beta^{3/2} (\beta^2 - 1)}{(1+z)^6} G_{12}(z). \quad (24)$$

This relation describes correctly properties of hot absorbers but decreases the column density of rare absorbers with $\delta_m \leq \delta_b$.

However, formation of weaker DM absorbers with $\beta \sim 1$ is accompanied by adiabatic inflow of baryons into the potential well. In this case, in accordance with the polytropic index $\gamma_b = 5/3$ for baryons, we can expect that

$$\delta_b \approx \beta^3, \quad \delta_m = \delta_0 \frac{q^2 (1+z)}{\beta^2 - 1} \geq \delta_b, \quad (25)$$

$$q \geq \beta^{3/2} (\beta^2 - 1)^{1/2} \delta_0^{-1/2} (1+z)^{-1/2},$$

where δ_0 was introduced in (21). This expression quantifies the bias between the compressed DM and baryonic components arising due to the impact of gaseous pressure (Jeans damping). For such absorbers we get from (22):

$$q \approx \left(\frac{N_{HI}}{2 \cdot 10^{16} \text{ cm}^{-2}} \right) \frac{G_{12} \delta_0}{\beta^{3/2} (1+z)^5}, \quad (26)$$

Both expressions, (24) and (26), define the dimensionless column density of DM component corrected for the impact of gaseous pressure. These relations can be successfully applied to absorbers formed due to adiabatic and strong shock compressions. However, the boundary between these limiting cases must be established *a priori*. So, to discriminate absorbers described by (24) and (26),

we can use a threshold Doppler parameter, β_{thr} , which, in fact, characterizes the Mach number of the inflowing matter. Thus, the weak adiabatically compressed absorbers can be conveniently separated with a threshold,

$$1 \leq \beta \leq \beta_{thr} \approx 1.5 - 2, \quad (27)$$

under condition (25) which can be reformulated as a restriction on the column density of neutral hydrogen, N_{HI} . Absorbers with $\beta \geq \beta_{thr}$ are considered as dominated by shock compressed gas and their DM column density is given by (24).

As was noted above, we cannot correctly determine properties of absorbers with $b \leq b_{bg}$ in the framework of our model because they violate the relation (21). However, we can consider them as adiabatically compressed, short lived unrelaxed and gravitationally unbound pancakes. Under these conditions absorbers with $b \leq b_{bg}$ can be described by the expression (26) which does not depend on b_{bg} .

As was found in Paper I, we can approximate the combined action of redshift variations of the UV background and random factors in expressions (24 & 26) by a two parameters relation

$$\langle G_{12}(z) \rangle \approx G_0(1 + \alpha_\gamma z), \quad (28)$$

where G_0 and α_γ are constants. The precision of this approach is moderate but a suitable choice of G_0 and α_γ provides a reasonable statistical description for majority of absorbers.

3.3. Statistical characteristics of absorbers

The model of absorbers discussed in this section is in fact independent from the statistical characteristics discussed in Sec. 2. It introduces the physically motivated combination of observed absorber characteristics, q , as given by (24) and (26), which can be compared with theoretical expectations introduced in Sec. 2. As it is shown in Sec. 5, the functions $\zeta(q, z)$ (11) and W_q found with this approach are consistent with expectations what verifies the interpretation of q as the DM column density of absorbers.

4. Mean characteristics of the observed sample

4.1. The database

In our analysis we use 14 high resolution QSO spectra listed in Table I. To decrease the scatter, we selected the sample of absorbers requiring that $10^{12}\text{cm}^{-2} \leq N_{HI} \leq 10^{15}\text{cm}^{-2}$, $b \leq 90$ km/s.

Absorbers with $b \leq b_{bg}$ must be excluded from the sample because for them the overdensity $\delta_b = (b/b_{bg})^{2/3} \leq 1$. For $b_{bg} = 16$ km/s our sample includes 3752 absorbers at redshifts $1.7 \leq z \leq 4$. Subpopulation of ~ 500 absorbers with $b \leq b_{bg}$ contains "artificial" caustics (McGill 1990) and absorbers which are most probably situated within regions where the average density and temperature are smaller than the values specified in (2) (Bi & Davidsen 1997; Zhang et al. 1998; Davé et al. 1999). As was noted above we can include them into consideration assuming that they are short lived gravitationally unbound pancakes.

For all models discussed in this paper we describe the redshift variations of the UV background intensity by the relation (28) with

$$G_0 = 12 - 15, \quad \alpha_\gamma = -0.22. \quad (29)$$

Estimates of the intensity of UV background through the proximity effect (Scott et al. 2000) give $\Gamma_{12} \approx 2 \pm 1$ at $z \sim 3$. Similar estimates were obtained in McDonald & Miralda-Escude (2001). These results are consistent with (23), (28) and (29) when

$$\langle \Theta_g \rangle \sim 0.4(b_{bg}/16\text{km/s})^{-7/2}.$$

Such a choice is in accordance with expectations of our model of absorbers and results in weak redshift variations of the function $\langle \zeta(z) \rangle$.

4.2. Redshift variations of absorbers characteristics

Here we consider the redshift variations of the observed parameters of absorbers, namely, the neutral hydrogen column density, $\log N_{HI}$, the Doppler parameter, b , and distances between absorbers

$$D_{sep} = \frac{c\Delta z_i}{H(z)} \approx 5.5 \cdot 10^3 \frac{\Delta z_i}{(1+z)^{3/2}} \sqrt{\frac{0.3}{\Omega_m}} h^{-1} \text{Mpc}. \quad (30)$$

For our sample of absorbers, the redshift variations of the mean observed parameters and the mean DM column density measured by the self similar variable, $\langle\zeta(z)\rangle$ (11), are plotted in Fig. 1 together with approximate fits :

$$\langle\zeta(z)\rangle \approx 0.73 \pm 0.08, \quad \langle b(z)\rangle \approx (31.9 \pm 1.6)\text{km/s}, \quad (31)$$

$$\langle\log N_{HI}\rangle \approx 13.2 \pm 0.22, \quad \langle D_{sep}\rangle \approx (2.5 - 0.6z)h^{-1}\text{Mpc}.$$

These results are consistent with the main results obtained in Paper I. It is interesting to notice that the redshift variations of $\langle\zeta(z)\rangle$ and $\langle b(z)\rangle$ plotted in Fig. 1 are clearly correlated.

The PDFs P_b , P_{HI} and P_{sep} , for the Doppler parameter, b , the hydrogen column density, N_{HI} , and the absorbers separation, D_{sep} , are plotted in Fig. 2 for three redshift intervals, namely, 1.7 – 2.5 (1357 lines), 2.5 – 3 (1235 lines) and 3 – 4.5 (1160 lines). This Fig. indicates that the shapes of PDFs weakly vary with redshift, what is consistent with the assumption that absorbers are long-lived and relaxed.

The mean values of the measured $\langle b \rangle$ and $\langle N_{HI} \rangle$ for these intervals of z are quite stable:

$$\langle b \rangle = 28.3\text{km/s}, \quad 31.1\text{km/s}, \quad 30.0\text{km/s},$$

$$\langle N_{HI} \rangle = 10^{13.5}\text{cm}^{-2}, \quad 10^{13.6}\text{cm}^{-2}, \quad 10^{13.8}\text{cm}^{-2}, \quad (32)$$

$$\langle D_{sep} \rangle = 1.75h^{-1}\text{Mpc}, \quad 1.34h^{-1}\text{Mpc}, \quad 0.94h^{-1}\text{Mpc}.$$

To quantify the redshift variations of the PDFs we calculate the mean values and dispersions of the relative differences,

$$c_i^k = [P_i^{(t)} - P_i^k] / [P_i^{(t)} + P_i^k],$$

between PDFs for the full sample ($P_i^{(t)}$, 3752 lines) and for each individual redshift interval (P_i^k , $k=1, 2, 3$), where $i = 1, 50$ numbers the bins with a step of 0.1 of the mean value. For the most representative first 25 bins $\langle c_i^k \rangle = 0$ with the standard deviation $\sigma_c \sim 0.1 - 0.15$.

These results indicate also the homogeneity of our sample. They confirm that the redshift evolution of the observed parameters of absorbers is very similar to the evolution of their mean values (31). It is an evidence in favor of the model of long-lived gravitationally confined absorbers. More detailed discussion of the observed spectra

can be found in Kim, Cristiani & D’Odorico (2002) and Kim et al. (2002).

It is interesting to estimate also the mean matter fraction accumulated by absorbers, $\langle f_m \rangle$. Rough estimates of f_m can be found by comparing the unperturbed mean size, $l_v \langle q \rangle$, with the mean separation of absorbers, D/N_{abs} for each individual spectrum, we get

$$\langle f_m \rangle \approx N_{abs} l_v \langle q \rangle / D \approx 0.87 \pm 0.14. \quad (33)$$

Here N_{abs} and D are the number of absorbers in the spectrum and its length along the line of sight. Averaging is performed over all fourteen spectra in our data base.

This value $\langle f_m \rangle$ exceeds the theoretical expectation $\langle f_m \rangle \sim 0.5 - 0.6$ at $z \sim 3$ (Paper I) what indicates a limited precision of this approach. In spite of this, it verifies that, in accordance with the physical model, at redshifts $z \leq 3$ at least half of matter could be accumulated by absorbers. This estimate does not contradict the observed Gunn–Peterson effect in HeII at $z \sim 3$ (Jacobsen et al. 1994) what indicates that essential fraction of baryons is homogeneously distributed. However quantitative estimates of this fraction strongly depends upon the intensity of UV background ionizing HeII.

5. Correlation function of the initial velocity field

In this Section we consider the cumulative and differential distribution functions, $W_q(\zeta)$ and $N_q(\zeta)$, and the correlation function of the initial velocity field, ξ_v , which can be found from $W_q(\zeta)$ as was described in Sec. 2.5. These functions depend upon several parameters which are known with limited precision. To test their influence we consider below three models of absorbers.

5.1. Three models of absorbers

Our results weakly depend upon the parameter β_{thr} introduced in Sec. 3.2 to separate absorbers formed by adiabatic and shock compression. The choice of β_{thr} is restricted by the shape of the function ξ_v at larger q (10) as $\beta_{thr} \leq 2$. In our model the amplitude of initial perturbations and

$$\tau_0 = 0.22, \quad \beta_{thr} = 1.5, \quad b_{bg} = 16\text{km/s}, \quad (34)$$

remain fixed. As is seen from (32), $\beta_{thr} \sim \langle b \rangle / b_{bg}$ and it turns out that $\sim 700 - 1000$ of absorbers in our sample have been adiabatically compressed. They form the left side of the PDF P_b plotted in Fig. 2 while richer absorbers with $\beta \geq \beta_{thr} \sim \langle b \rangle / b_{bg}$ have been presumably formed by merging and shock compression.

The cumulative and differential distribution functions depend also upon the survival probability, $W_s = \text{erf}^n(\sqrt{\zeta})$, (14, 15) described by the power index n . Finally, of course our results depend upon the number of absorbers in the sample, N_{smp} , used in the analysis. In particular, in spite of the relatively small number of absorbers with $b \leq b_{bg}$ when they are included they noticeably change the correlation function ξ_v .

To test the influence of these factors we consider three models with parameters:

$$n = 1, \quad N_{smp} = 3752, \quad G_0 = 12.5, \quad (35)$$

$$n = 1, \quad N_{smp} = 4248, \quad G_0 = 12.5, \quad (36)$$

$$n = 2, \quad N_{smp} = 4248, \quad G_0 = 15.5, \quad (37)$$

for the Model 1, Model 2 and Model 3, respectively. Parameter G_0 was introduced in (28) to characterize the intensity of the UV background. The Model 1 includes only absorbers with $b \geq b_{bg}$ whereas Models 2 & 3 include also absorbers with $b \leq b_{bg}$ and differ by the choice of survival probability, W_s , and the intensity of the UV background.

5.2. Cumulative PDFs for dimensionless DM column density

As was discussed in Sec. 2.5, the observed cumulative distribution function, $W_q(> q/\tau)$, can be estimated using q/τ obtained from our sample of observed absorbers with the model described in Sec. 3 and parameters (34-37). For these models the correlation function ξ_v is well fitted by the expression

$$\xi_{fit} = 1 - 1.5q \sqrt{\frac{q^2 + p_1^2}{q^2 + p_2^2}}, \quad 0.5 \geq q \geq 10^{-3}, \quad (38)$$

$$p_1 = 1.3 \cdot 10^{-2}, \quad p_1 = 10^{-2}, \quad p_1 = 2 \cdot 10^{-3},$$

$$p_2 = 7 \cdot 10^{-4}, \quad p_2 = 4 \cdot 10^{-3}, \quad p_2 = 2 \cdot 10^{-3},$$

for the Model 1, Model 2, and Model 3, respectively. The function (38) becomes identical with the reference correlation function (10) ξ_{CDM} for $q \geq p_1 \geq p_2$.

The measured functions W_q for the three models are plotted in Fig. 3 together with fits (14) and (15) for ξ_v given by (38) and with a scatter $\propto 2/\sqrt{N_{abs}}$ where N_{abs} is the number of absorbers in each bin. The difference between the measured and fitted functions W_q is characterized by the relations:

$$W_q \approx \begin{cases} (0.96 \pm 0.2)\text{erf}^2(\sqrt{\zeta}), & \chi^2 = 0.5, \\ (1.0 \pm 0.1)\text{erf}^2(\sqrt{\zeta}), & \chi^2 = 0.2, \\ (1.1 \pm 0.2)\text{erf}^3(\sqrt{\zeta}), & \chi^2 = 0.5, \end{cases} \quad (39)$$

where ζ is given by (11) and (38). χ^2 is found for ratios of measured and fitted $W_q/\text{erf}^{n+1}(\sqrt{\zeta})$ for 26 measured points. For ξ_v given by (38) all fits are reasonably consistent with the measured W_q .

5.3. Differential PDFs for dimensionless DM column density

For all three models the differential PDFs were found from measured q and τ with ξ_v given by (38). These PDFs are quite sensitive to the functions ξ_v and W_s , what allows one to check the correctness of the choice of these functions.

The differential PDF, $N_q(\zeta) = \langle \zeta \rangle dW_q/d\zeta$, is plotted in Fig. 4 for the Model 1, Model 2, and Model 3 together with the fit

$$N_q(\zeta) \approx \frac{(n+1)\langle \zeta \rangle}{\sqrt{\pi}} \exp(-\zeta) \frac{\text{erf}^n(\sqrt{\zeta})}{\sqrt{\zeta}}. \quad (40)$$

This expression fits well the observed PDF for

$$\langle \zeta_{th} \rangle \approx \langle \zeta \rangle = 0.85, \quad 0.87, \quad 1.15, \quad (41)$$

for Models 1, 2, & 3, respectively. Here $\langle \zeta_{th} \rangle = 0.82$ & 1.05 are the mean values for N_q (40) with $n = 1$ and $n = 2$. For $\zeta \leq 0.2\langle \zeta \rangle$ the measured PDF becomes sensitive to the possible incompleteness of the sample.

The concordance of the measured and expected PDFs can be also checked by the Kolmogorov-Smirnov test. For the three models plotted in Fig. 4 the cumulative PDFs are consistent with $\text{erf}^{n+1}(\sqrt{\zeta})$ with probabilities

$$P_{KS} = 0.78, \quad P_{KS} = 0.76, \quad P_{KS} = 0.47, \quad (42)$$

respectively. These results confirm, for a given set of DM column density, a close link between the accepted survival probability, W_s , and the measured correlation function, ξ_v . For $\zeta \geq \langle \zeta \rangle$ the exponential shape of the function N_q coincides with its theoretically expected shape for Gaussian initial perturbations and the CDM-like power spectrum (10), (11), (14).

5.4. Correlation function of the initial velocity field

As was described in Sec. 2.5 we can derive the correlation function of the initial velocity field, $\xi_v(q)$, by solving Eq. (18). This function depends on both the survival probability, W_s , and the sample of absorbers (see 34-37).

For all three models, the measured correlation functions $\xi_v(q)$ are plotted in Fig. 5 together with ξ_{fit} (38) and with the correlation function ξ_{CDM} (10). For all models variations of the ratios of measured and fitted functions, $(1 - \xi_v)/(1 - \xi_{fit})$, are quite moderate and are quantified as follows:

$$(1 - \xi_v)/(1 - \xi_{fit}) \approx 1 \pm 0.2, \quad 0.3 \geq q \geq 10^{-3}, \quad (43)$$

$$\chi^2 = 0.9, \quad 0.4, \quad 0.7,$$

for the Model 1, Model 2 and Model 3, respectively. Here χ^2 are found from 26 measured points. This fact confirms the self consistency of our models and the choice of parameters (29) and (34-37).

At the same time, at larger scales, $0.3 \geq q \geq 0.03$, $10h^{-1}\text{Mpc} \geq l_{vq} \geq 1h^{-1}\text{Mpc}$, for all three Models the differences between the measured and CDM-like correlation functions are negligible

$$(1 - \xi_v)/(1 - \xi_{CDM}) \approx 1 \pm 0.15, \quad \chi^2 = 0.2, \quad (44)$$

where χ^2 are found for the ratios $(1 - \xi_v)/(1 - \xi_{CDM})$ for 14 measured points. These results demonstrate that for such scales the differences between the CDM-like initial power spectrum and the measured one do not exceed 15%.

However, at small scales all measured correlation functions differ from the ξ_{CDM} (10). Quantitatively these differences are characterized by the χ^2_{CDM} found for the ratios $(1 - \xi_v)/(1 - \xi_{CDM})$ for 26 measured points. For the Model 1, Model 2 and Model 3 we get, respectively :

$$\chi^2_{CDM} = 550, \quad \chi^2_{CDM} = 120, \quad \chi^2_{CDM} = 33. \quad (45)$$

These results show that this difference between the measured ξ_v and ξ_{CDM} decreases when formation of pancakes with small mass is suppressed more strongly i.e. when the survival probability is $W_s = \text{erf}^2(\sqrt{\zeta})$.

6. Redshift distribution of absorbers

The redshift distribution of absorbers only weakly depends on the properties of weaker absorbers because they are relatively rare, only about $\sim 20\%$ of absorbers have $q \leq 0.03$. It depends mainly upon measured redshifts of absorbers and is only weakly sensitive to the physical model of absorbers discussed in Sec. 3. This means that it is an important independent test of the model of absorbers formation considered in Sec. 2.

The redshift distribution of absorbers is quite well fitted by the relation (16) which is applied to all samples of absorbers with $q_{thr} \geq q_0$. To illustrate this property we plot in Fig. 6 the measured function $\langle n_{abs}(z) \rangle$ for all 4250 absorbers together with two fits (16).

As was described in Paper I, for each redshift interval, $\Delta z = 0.1$, all absorbers were organized into an "equivalent single field" by arranging them one after the other along the line of sight. The mean number density of absorbers, n_{abs} , and its scatter were found by comparing the equivalent single field with a corresponding Poissonian distribution. The measured function n_{abs} is plotted in Fig. 6 together with the best fits (16) for Model 1 and Model 3. Both fits are very similar to each other what demonstrates that the observed redshift distribution of absorbers only weakly depends on the shape of the initial power spectrum. However, the observed redshift distribution of absorbers verifies the Gaussianity of the initial perturbations since it is manifested in the characteristics of the Ly- α forest.

7. Reliability and precision of our estimates

To measure the initial power spectrum it is necessary to use a model of absorbers which links the observed Ly- α clouds with the DM spatial distribution. The model introduced in Secs. 2 & 3 provides a quite reasonable and self consistent statistical description of the basic properties of ab-

sorbers (Paper I and Secs. 4 & 5). For the three models under consideration the measured correlation function of the initial velocity field, ξ_v , is consistent with the CDM-like one for $q \geq 0.03$, what verifies the reliability of our approach.

However, at small scales ($q \leq 0.03$) the measured function ξ_v differs from the CDM-like one. These differences are caused by the deficit of absorbers with small q/τ & q and, therefore, it can be artificially enhanced by an action of several factors. The most important ones are the possible incompleteness of the observed sample of weaker absorbers, overestimates of the DM column density by our model of absorbers (24, 26), and the choice of the survival probability (14, 15).

Usual estimates of the possible incompleteness of the sample ($\leq 20\%$) are based on the quality of the observed spectra but for compiled samples of absorbers such estimates are not reliable. The best way to test the influence of this factor is to repeat the analysis with a richer sample of observed absorbers.

By comparing the Model 1 with the Model 2 we test the sensitivity of our results to variations of the observed sample. In spite of the fact that the condition $b \leq b_{bg}$ is satisfied only by a relatively small fraction of absorbers (≈ 500) their influence is quite significant because when they are included they almost double the number of weaker absorbers. In particular, the difference between the measured ξ_v and the reference one (10) is reduced by half but it is not eliminated. As is seen from (45), this difference remains clearly noticeable even for the Model 3 for which both factors, larger number of absorbers and larger power index, $n = 2$, of the survival probability work together to decrease this difference.

On the other hand, extension of the sample by adding 355 absorbers with $10^{13}\text{cm}^{-2} \leq N_{HI} \leq 10^{15}\text{cm}^{-2}$ from published spectra of four quasars (2126-158, Giallongo et al. 1993; 1700+642, Rodrigues et al. 1995; 1225+317, Khare et al. 1997; 1331+170, Kulkarni et al. 1996) does not change our previous results (43, 45). This test demonstrates that the measured velocity correlation function strongly depends on the representativity of the sample of weak absorbers and estimates of their Doppler parameter but it only weakly depends on the sample of stronger absorbers.

Our choice of the survival probability in the expression (14) is based on the measured distribution of walls in observed galaxy surveys and in simulations rather than on theoretical arguments. Comparison of results obtained with the expressions (14 & 15) illustrates the importance of this factor and shows that the measured velocity correlation function could be noticeably different from that derived in a standard way from the CDM-like power spectrum only for a moderate survival probability, $W_s(q, \zeta)$. The analysis repeated for a wider set of functions $W_s(q, \zeta)$ confirms that the measured functions W_q and N_q strongly restrict the acceptable shape of the survival probability, but for a suitable choice of W_s , the difference between ξ_{CDM} and the measured velocity correlation function becomes moderate.

These results show that the merging of low mass pancakes is an important factor and it should be thoroughly investigated. As the first step of such investigation the PDFs N_q were measured for three sets of DM walls selected at $z = 0$ with a small threshold richness from two standard high resolution simulations (Cole et al. 1998; Jenkins et al. 1998). These PDFs are plotted in Fig. 7 together with fits (14). As is seen from this Figure, in all the cases there is a noticeable excess of low mass objects. It can be related to the expected disruption of compressed DM walls into a system of high density clouds, what decreases the observed pancake column density. These results favor a moderate survival probability of low mass absorbers. However, such analysis should be continued with more precise simulations.

As was noted in White & Croft (2003) the formation of LSS elements is accompanied by their partial disruption and creation of low mass clouds. This process is more important for formation of galaxies and their low mass satellites what was also discussed in DD02 and Paper I. This process can increase the fraction of low mass absorbers in comparison with theoretical expectations, what, however, can only partially suppress distortions of the initial power spectrum considered in this paper.

This discussion confirms that quantitative estimates of the shape of the function ξ_v at small scales actually depend upon the sample used in the analysis and the model linking the observed absorber characteristics with their DM column den-

sity and the correlation function ξ_v . However, differences between the measured and the CDM-like correlation functions remain quite significant for a wide range of models.

By analyzing the distribution of Lyman- α clouds we can test the initial power spectrum of perturbations to unprecedentedly small scale and both outcomes confirmation of the CDM-like shape of the power spectrum or detection of distortions are equally important. Results of such analysis can be improved with a more detailed numerical simulations and a richer sample of observed absorbers.

8. The initial power spectrum

For larger scales, $q \geq 0.1$, our approach describes reasonably well the properties of richer absorbers and our analysis verifies the CDM-like shape of the correlation function ξ_v and the initial power spectrum (3). The correlation function ξ_v is well fitted by the one parameter relation (10), where the parameter q_0 is expressed through the spectral moments, m_0 and m_{-2} (6), and it depends upon the mass of dominant DM particles. For $M_{DM} \approx 3 - 5$ keV, $q_0 \approx (1 - 0.7) \cdot 10^{-2}$ is expected.

However, at small scales the shape of the observed correlation function ξ_v differs from the CDM-like one (10), what indicates a more complicated shape of the initial power spectrum at small scale. The initial power spectrum can be restored from the function ξ_v . Using (9) we obtain

$$P(\eta) \propto \int_0^\infty dq q \xi(q) \left[\sin(q\eta) + 2 \frac{\cos(q\eta)}{q\eta} \right] \quad (46)$$

The precision and reliability of our estimates are however limited (Sec. 7) and we measure the function $\xi(q)$ only in limited range of q . So, here we will present only examples of spectra which generate the correlation functions ξ_v similar to the measured one. As was noted in Sec. 3, the expressions (24) and (26) define the DM column density corrected for the Jeans damping and therefore as a reference we consider the standard normalized spectrum (3) for the mass of dominant fraction of DM particles $M_{DM} = 3$ keV, $q_0 = 0.01$:

$$Q(\eta) = \eta T^2(\eta) D_W(\eta), \quad \eta = k/k_0, \quad D_J(\eta) = 1. \quad (47)$$

Distortions of the spectrum (47) are described by:

$$\Delta Q(\eta) = \frac{A_p}{\sqrt{2\pi}\sigma_p} \exp[-0.5(\eta - \eta_p)^2/\sigma_p^2], \quad (48)$$

$$A_p = 5 \cdot 10^{-2}, \quad \eta_p = 170, \quad \sigma_p = 65, \\ A_p = 2.8 \cdot 10^{-2}, \quad \eta_p = 170, \quad \sigma_p = 280,$$

for Model 1 and Model 3, respectively. The correlation functions ξ_v generated by the spectra (47) and (48) and these spectra are plotted in Fig. 8 and Fig. 9.

The interpretation of these distortions is not unique because of very limited available information. We can estimate the function ξ_v only at $q \geq 10^{-3}$ where its dependence upon the mass of DM particles is moderate and even for $M_{DM} \geq 10^4$ keV it increases of about 1.5 times only. This means, for example, that even so essential increase of M_{DM} cannot provide noticeable effects and the most probable source of the observed distortions are adiabatic or, perhaps, isocurvature perturbations predicted by some models of the early Universe and inflation.

Recent WMAP measurements confirmed that as expected adiabatic perturbations dominate on large scale (Peiris et al. 2003) and that they are Gaussian (Komatsu et al. 2003). However, these results do not preclude the existence of distortions of the standard CDM-like power spectrum at small scales due to both adiabatic and isocurvature perturbations (Peiris et al. 2003).

The measured distortions of the power spectrum can be considered as an observational evidence in favor of the one field inflation with a complicated inflation potential (see, e.g., Ivanov, Naselsky & Novikov 1994) or multiple fields inflation (see, e.g., Polarski & Starobinsky 1995; Turok 1996). Both models generate adiabatic or isocurvature deviations from the simple CDM-like power spectrum. More detailed discussion of such models can be found, for example, in Peiris et al. (2003).

9. Summary and Discussion.

In this paper we continue the analysis of a sample of ~ 4500 observed absorbers initiated in Paper I and based on the statistical description of Zel'dovich pancakes (DD99, DD02). This approach allows one to connect the observed characteristics of absorbers with fundamental properties

of the initial perturbations and demonstrates the common origin of absorbers and the Large Scale Structure observed in the spatial galaxy distribution at small redshifts.

The physical model of absorbers proposed in Paper I and essentially improved in Sec. 3 links three observed characteristics of the Lyman- α clouds, namely, the redshift, z , the Doppler parameter, b , and the column density of neutral hydrogen, N_{HI} , with the DM and baryonic column densities, overdensity and entropy. It describes redshift dependence of the observed characteristics of absorbers discussed in Sec. 4, discriminates between the random and regular variations of absorbers characteristics and allows one to obtain a reasonable statistical description of these characteristics. It also explains the observed redshift variations of the linear number density of absorbers and links them with the fundamental parameters of the initial power spectrum.

Such a complex approach allows one to test its self consistency through the comparison of several measured statistical characteristics with corresponding theoretical expectations. As was shown above, it also allows one to test the shape of the correlation function of the initial velocity field and of the initial power spectrum on unprecedently small scale.

The progress achieved demonstrates again the key role of the representativity and completeness of the observed samples for the construction of the physical model of absorbers and reveals a close connection between the observational database and obtained results. Some of the most interesting results were derived from the distribution of weak absorbers but unfortunately the available sample of such absorbers has only limited statistical significance. Further progress can be achieved with a richer sample of observed absorbers and by testing our approach on a more representative numerical simulations.

9.1. Main results

Main results of our analysis can be summarized as follows:

1. We demonstrate that the physical model of absorbers proposed in Paper I and Sec. 3 is self consistent and agrees well with the basic observed characteristics of the Lyman- α

clouds. This fact indicates that the majority of absorbers can be considered as long-lived, gravitationally bound and relaxed.

2. Using the Zel'dovich theory of gravitational instability we link the PDF of DM column density found for the observed sample of Lyman- α clouds with the correlation function of the initial velocity field, ξ_v , what allows one to estimate the initial power spectrum to unprecedently small scale.
3. We found that at larger scales both the measured function ξ_v and the initial power spectrum of perturbations do not differ by more than ~ 10 – 15% from the predictions of the CDM model. This result confirms the basic predictions of the inflationary scenario.
4. At scales $\sim 30 - 300h^{-1}\text{kpc}$ we see noticeable differences between the measured correlation function ξ_v and the expected one for the CDM-like power spectrum. These differences can be considered as an observational evidence in favor of a more complex inflation, which generates an excess of power at small scales. In turn, this excess of power accelerates the formation of first galaxies and causes early reheating of the Universe.
5. Our quantitative estimates depend upon the limited statistics of weak absorbers and their poorly known survival probability. However, both confirmation of CDM-like shape of the initial power spectrum or detection of its distortions are equally important.

These results indicate that the proposed approach is quite promising and the analysis should be continued with a richer sample of observed Ly- α absorbers. Application of this approach to simulated matter distribution at $z = 0$ and to the sample of $\sim 100\,000$ galaxies compiled in the SDSS DR1 demonstrates its high efficiency for the quantitative description of strongly nonlinear matter condensations. However, its application for the Ly- α forest at high redshifts needs to be directly tested with a representative numerical simulations what, in turn, will allow to improve the estimates of the initial power spectrum.

9.2. Physical model of absorbers

The physical model of absorbers introduced in Paper I and improved in Sec. 3 links the measured z , b and N_{HI} with other physical characteristics of both gaseous and DM components forming the observed absorbers. In this model we consider the majority of absorbers as long-lived gravitationally bound and partly relaxed objects formed in the course of both linear and nonlinear condensation of the DM component. The existence of galaxies and quasars at high redshifts and the observed reheating of the Universe at redshifts $z \geq 6$ demonstrate the importance of nonlinear processes at redshifts under consideration. Numerous simulations (see, e.g., Frenk 2002) also confirm the formation of high density DM filaments and sheets at these redshifts.

The Zel'dovich theory of gravitational instability indicates the self similar character of the processes of DM structure formation and allows formation of numerous high density relaxed DM filaments and sheets already at high redshifts. Their typical sizes and their mass function depend upon the initial power spectrum and their mean characteristics progressively change with time. However, the DM structure at high redshifts is expected to be qualitatively similar to the one observed at small redshifts. The Ly- α clouds trace this DM structure and, as was shown in Sec. 4, the PDFs of their observed characteristics only weakly depend on the redshift.

For low mass pancakes the spatial distribution of the baryonic and DM components can be strongly biased due to the influence of the gaseous pressure (Jeans damping). The physical model of absorbers considered in this paper allows for this bias.

Our approach is consistent with the weak redshift variations of the mean observed characteristics of absorbers, namely, $\langle b \rangle$ and $\langle N_{HI} \rangle$, and even the shape of their distribution functions (Sec. 4) does not change with time. Moreover, the main statistical characteristics of absorbers discussed in Paper I and in Secs. 4 & 5 coincide with theoretical expectations. In particular, the redshift variations of $\langle \zeta \rangle$ do not exceed 10% (Sec. 4), the mean value of ζ and its measured PDF coincide with the expected ones (Sec. 5.3). The same approach allows one to describe the redshift variation of the linear

number density of absorbers (Sec. 6).

Analysis of the main characteristics of absorbers performed in Paper I shows that the sample of observed absorbers can be composed of DM pancakes with complex evolutionary histories. They can be formed due to merging of earlier formed pancakes or compression of background matter, and both adiabatic, for $\beta \leq 2$, and shock compressions, for $\beta \geq 2$ are equally possible. The great diversity of these histories is clearly seen already from the well known broad distribution of absorbers in the " $b - N_{HI}$ " plane (see, e.g., Hu et al. 1995).

Properties of absorbers are changing even after formation of gravitationally bound pancakes. In Paper I we discussed five most important factors that determine absorbers evolution after formation. They are: the transverse expansion and/or compression of pancakes, their merging, the radiative heating and cooling of compressed gas, and disruption of pancakes into a system of high density clouds. To illustrate the influence of these factors and correlations between different characteristics of absorbers we roughly discriminated in Paper I three subpopulations of absorbers with various entropies and overdensities.

Our approach allows one to discriminate between the systematic and random variations of properties of absorbers. The former ones are naturally related to the progressive growth with time of the DM column density of absorbers, $q(z)$, what can be described theoretically. The action of random factors cannot be satisfactory described by any theoretical model. However, in the framework of our approach, the joint action of all random factors can be described by one random function, which can be identified with the entropy of the compressed gas and it is directly expressed through the observed parameters (Paper I).

9.3. Reconstruction of the initial power spectrum

Naturally, the formation and further evolution of DM pancakes is determined by the initial power spectrum. However, the great diversity of their evolutionary histories makes the reconstruction of this spectrum from observations of the Ly- α forest difficult. In this paper we solve this problem in the framework of the complex statistical investiga-

tion of absorbers that allows one to check the self consistency of this approach. In spite of this, our results are based on some assumptions and, so, are model dependent. To check and to improve this approach we have to apply it to the high resolution representative simulations of formation of galaxies and absorbers.

This statistical description connects the PDF of the DM column density of pancakes with their survival probability, W_s , and the correlation function of the initial velocity field, ξ_v . For Gaussian initial perturbations and for a given W_s , this connection allows one to reconstruct the approximate shape of the function ξ_v and to reveal its possible divergence from the expected one for the CDM-like initial power spectrum corrected for damping due to a finite mass of DM particles. In turn, this divergence can be interpreted as an indication of existence of special features in the initial power spectrum at small scales.

In our approach we use the measured PDF of the DM column density of pancakes rather than the smoothed density field. It therefore avoids the complicated problem of density variations along the line of sight and mass conservation. It does not depend on the peculiar velocity of absorbers and is not restricted by the Nyquist limit and the distances between absorbers. So, this indirect approach allows one to check the shape of the initial power spectrum in the real space up to unprecedently large wave numbers, $\eta = k/k_0 \sim 100$.

For larger scales, $\geq 1 - 2h^{-1}$ Mpc, $\eta \leq 3$, our analysis verifies the CDM-like shape of the initial power spectrum and the correlation function ξ_v . However at small scales noticeable differences between the CDM-like and measured spectra are detected. The reliability of these differences is problematic (see Sec. 7) but both confirmation and/or elimination of these distortions are equally important.

9.4. Numerical simulations and the model of "fluctuating Gunn-Peterson approximation"

The leading role of numerical simulations in investigation of the LSS is well known. They clarify many problems of structure formation and evolution at all redshifts and, in particular, link the observed characteristics of absorbers with those that

are not directly observable. This link allows one to test the physical model of absorbers and, further on, to use it to recover the density fields and the initial power spectrum from the observed Ly- α forest. Here we shortly compare our results with numerical simulations.

9.4.1. The model of "fluctuating Gunn-Peterson approximation"

One of the popular model of the observed Ly- α forest is the "fluctuating Gunn-Peterson approximation" (FGPA) widely discussed during the last five years (see, e.g., Croft et al. 1998, 2002; Nusser & Haehnelt 2000; McDonald et al. 2000; Phillips et al. 2001; Zaldarriaga, Hui & Tegmark 2001; Shaya et al. 2002). It is focused on the connection between the observed redshift variations of the flux emitted from quasars and the initial power spectrum.

In this approach absorbers are considered as formed by a mildly nonlinear unshocked compression of the background matter. It links absorption lines with large diffuse gaseous clouds with moderate overdensities which are expanded by the residual Hubble flow. For such clouds their velocity profile depends mainly on their size, while the thermal broadening is considered as minor (Croft et al. 2002). However, other authors consider this broadening as quite essential (see, e.g., Meiksin, Bryan & Machacek 2001; White & Croft 2003).

The main result of the FGPA is the determination of the power spectrum. This method does not use the observed hydrogen column density and the Doppler parameter. It begins with the analysis of the measured one dimensional spectrum of the flux and converts it into the power spectrum of the matter. The nonlinear effects are partly taken into account when the measured flux spectrum is converted to the matter spectrum with the special function $b(k)$ (Croft et al. 2002). This simple method, in spite of its deficiencies, surprisingly well restores the CDM-like power spectrum down to scales $\sim 1h^{-1}$ Mpc.

The application of the FGPA is restricted by the Nyquist limits. For the typical separation of observed absorbers (32)

$$\langle D_{sep} \rangle \approx 1 \left(\frac{0.2}{\Omega_m h} \right) h^{-1} \text{Mpc}, \quad (49)$$

the analysis allows one to reach a typical wave

number

$$k_N \approx \frac{\pi}{2D_{sep}} \approx 1.6 \left(\frac{\Omega_m h}{0.2} \right) h\text{Mpc}^{-1}, \quad \eta_N = \frac{k_N}{k_0} \approx 8.$$

At such scales, the similarity of the observed spectra with the CDM-like one is confirmed by our results (44).

Comparison of simulated and measured flux characteristics in McDonald et al. (2000) shows an excellent agreement. However, later analysis revealed systematic inconsistencies between the observed and simulated intermittent features of the flux that indicates the underestimation of nonlinear evolution in simulations (Pando et al. 2002). White & Croft (2003) note also the importance of the non-linearity of matter clustering for the reconstruction of the power spectrum.

The FGPA has been criticized, for example, by Zaldarriaga, Scoccimorro & Hui (2002) who notice the limited usefulness of available simulations, limitations of the inversion technique and the importance of nonlinear effects. The same problems are also discussed in Gnedin & Hamilton (2002), Tegmark & Zaldarriaga (2002) and Seljak, McDonald & Makarov (2003).

9.4.2. Properties of simulated forest

Usually the comparison of observed and simulated characteristics of the Ly- α forest is restricted by the flux emitted from quasars but always they are found to be quite consistent. However, the flux integrates the HI distribution over absorber and therefore it does not characterize it uniquely.

More detailed comparison of the Doppler parameter, b , and the column density of neutral hydrogen, N_{HI} , performed in Meiksin, Bryan & Machacek (2001) reveals that no simulations provide a statistically acceptable match to the observed b and N_{HI} distributions. In particular, they found that the median measured Doppler parameters exceed the simulated one by as much as 30 – 60% especially for optically thin lines and also the simulated and measured N_{HI} distributions tend not to agree. It can be expected that results presented in Sec. 4.2 enhance divergences between the simulated and observed *quantitative* characteristics of the forest.

As was noted in Paper I, for the sample dominated by recently formed ‘young’ absorbers a

strong redshift evolution of observed characteristics and, in particular, of the Doppler parameter, is expected. Perhaps, this effect enhances distortions between measured and simulated Doppler parameters.

The available numerical simulations are restricted by technical limitations but, in spite of this, they could help to solve many unclear problems of the early structure formation. First of all, it is link between the gaseous and DM components and estimate of the degree of nonlinearity. A detailed description of the DM distribution is now possible with at least two effective methods – the Minimal Spanning Tree (Demiański et al. 2000; Doroshkevich et al. 2001) and the Minkowski Functional (see, e.g., Schmalzing et al. 1999) techniques. Characteristics of DM distribution are extremely important for the reconstruction of the processes of formation of the Ly- α forest. These characteristics can be directly compared with expectations of the Zel’dovich theory discussed in Sec. 2.

Now it is not clear why the FGPA links the Ly- α forest with large diffuse gaseous clouds with moderate overdensities and why the high overdensity DM pancakes – relaxed or unrelaxed – are not seen in simulations. It is natural to expect that the formation of galaxies is accompanied by formation of numerous high overdensity pancakes. Simple estimates show that, for parameters discussed in Sec. 4.2, the one dimensional collapse leading to formation of high density pancakes is quite probable at all redshifts under consideration. For $\langle b \rangle / b_{bg} \geq \beta_{thr}$ shock compression dominates.

It is also not clear what happens with the formed DM clouds in the course of their further evolution and why merging of pancakes is suppressed. It is one of the important processes responsible for evolution of the structure which is clearly seen in numerous high resolution simulations performed in large boxes. This process is accompanied by shock compression of the gas and an essential growth of its entropy. In turn, variations of the entropy explain the strong scatter of absorbers in the “ $b - N_{HI}$ ” plane (Hu et al. 1995). This list of questions can be substantially extended.

To achieve the required resolution, the simulations of the forest are usually performed in relatively small boxes with sizes $L_{box} \sim 5 - 20 h^{-1} \text{Mpc}$

what eliminates the large scale initial perturbations. To test how accurately such numerical simulations reproduce observations in Fig. 10 we compare the velocity correlation function ξ_v for CDM power spectrum with velocity correlation functions for two truncated spectra used in simulations. As is seen from this Figure, both correlation functions derived from truncated spectra at scales $l_v q k_0 \geq 0.4$ are suppressed. This in turn slows down the merging of clouds, decelerates the formation of richer absorbers and distorts their other characteristics. As was found in Secs. 4.2 and 5.3, for the cosmological model (1) the mean size of compressed absorbers is

$$l_v k_0 \langle q(z) \rangle \approx \frac{1.1 l_v k_0 \langle \zeta \rangle}{(1+z)^2} \approx 0.4 \left(\frac{4}{1+z} \right)^2, \quad (50)$$

what coincides with the critical value found above.

This estimates indicate that in simulations performed with $k_0 L_{box} \leq 5 - 6$ the formation of richer absorbers with $q \geq \langle q(z) \rangle$ is strongly suppressed and the weaker adiabatically compressed absorbers dominate. On the other hand, estimates discussed in Sec. 4.2 verify that at redshifts under consideration at least half of matter could be already accumulated by absorbers and, so, their evolution could be driven by the processes of merging and shock heating. These inferences should be tested on simulated DM characteristics of pancakes and compared with expected ones for the corresponding power spectrum, for example, with methods described in Sec. 2.

9.4.3. Measurements of the power spectrum

The FGPA picture seems to be quite different from our representation of absorbers as a network of discrete gravitationally bound pancakes with a variety of overdensities. Our model identifies the Doppler parameter with the depth of the DM potential well and the temperature of compressed gas rather than with the residual expansion of matter. It assumes domination of long lived absorbers what agrees well with results obtained in Sec. 4.2. Direct estimates obtained with the pancake sizes and Doppler parameters specified in this section show that the formation of such high density absorbers is quite probable at all redshifts under consideration.

Both models describe quite well some of the observed properties of the Lyman- α forest but

they differ in emphasizing domination of discrete or diffuse absorbers. In many respects they are complementary to each other because diffuse and discrete absorbers coexist and fractions of these types of absorbers change with redshift. Evidently the diffuse absorbers dominate just after reheating while discrete absorbers dominate at lower redshifts. These differences demonstrate the complex character of the Lyman- α absorption clouds and indicate that both models should be improved after detailed analysis of truly representative simulations of the forest.

The proposed here method of measuring the power spectrum is based on the strong connection between the power spectrum and the mass function of absorbers and seems to be quite promising. It is not restricted by the Nyquist limit and therefore it can be extended to scales about ten – thirty times smaller than the method based on the FGPA. It is not rigidly linked to the accepted physical model of absorbers which can be corrected and improved in the course of further investigations. It can be also easily generalized for more refined relations between the mass function and correlation function of velocity field. These corrections can be introduced after detailed investigations of improved and truly representative simulations which reproduce *all* observed characteristics of the Ly- α forest and link them with DM characteristics of pancakes.

9.5. Reheating of the Universe and the initial power spectrum

Recent observations of high redshift quasars with $z \geq 5$ (Djorgovski et al. 2001; Becker et al. 2001; Pentericci et al. 2001; Fan et al. 2001, 2003) provide a clear evidence in favor of the reionization of the Universe at redshifts $z \sim 6$, when the volume averaged fraction of neutral hydrogen is found to be $f_H \geq 10^{-3}$ and the photoionization rate $\Gamma_\gamma \sim (0.2 - 0.8) \cdot 10^{-13} \text{s}^{-1}$. These data coincide with those expected at the end of the reionization epoch which probably took place at $z \sim 6$. On the other hand, recent WMAP data shift the redshift of reionization up to $z \sim 20 \pm 10$ (Kogut et al. 2003), what implies a complex ionization history.

The reionization at $z \sim 6 - 10$ is consistent with the CDM-like power spectrum with the mass of dominant DM particles $M_{DM} \sim 1 - 5 \text{ keV}$ (see

discussion in Paper I). Earlier reionization is compatible with a larger mass of the dominant fraction of DM particles, $M_{DM} \geq 1$ MeV or with distortions of the CDM-like initial power spectrum at small scales, what in turn implies a complex inflation and a more efficient formation of galaxies at high redshifts (see discussion in Spergel et al. 2003).

Models with complex inflation and an excess of power at small scales were recently discussed in connection with distortions of the CMB polarization (Naselsky & Novikov 2002; Doroshkevich, Naselsky I., Naselsky P., Novikov 2003) and galaxy formation (Sommer-Larsen et al. 2003). This means that measurements of the initial power spectrum at small scale are important for many aspects of modern cosmology.

The future Planck mission will provide high accuracy measurements of the CMB polarization and clarify the ionization history of the Universe. However, these results will give again only indirect information about the possible distortions of the power spectrum. This means that the measurement of such distortions with the Ly- α forest remains the most efficient way for investigation of the initial power spectrum at small scale.

The preliminary estimates obtained above seem to be quite promising but must be tested with richer samples of observed absorbers. Such investigations will allow one to obtain more detailed and reliable information and better understanding of the physical processes at high redshifts and the shape of the initial power spectrum.

Acknowledgments

AGD is grateful to Dr. S. Cristiani and Dr. T.S.Kim for the permission to use the unpublished observational data. This paper was supported in part by Denmark's Grundforskningsfond through its support for an establishment of Theoretical Astrophysics Center and by a grant of the Polish State Committee for Scientific Research. MD wants to thank TAC for great hospitality and support. AGD also wishes to acknowledge support from the Center of Cosmo-Particle Physics, Moscow. Furthermore, we wish to thank the anonymous referee for many useful comments.

REFERENCES

- Bardeen J.M., Bond J.R., Kaiser N., Szalay A., 1986, *ApJ.*, 304, 15 (BBKS)
- Barkana R., Haiman Z., Ostriker J.P., 2001, *ApJ.*, 558, 482
- Becker R.H. et al. 2001, *AJ*, 122, 2850
- Bergeron J., Cristiani S., & Shaver P.A., 1992, *A&A*, 257, 417
- Bi H., & Davidsen A.F., 1997, *ApJ.*, 479, 523
- Bond R., Wadsley J.W., 1997, in "Structure and Evolution of the IGM from QSO Absorption Line Systems", Eds. P.Petitjean, S.Charlot, Editions Frontiers, Paris, p. 143
- Bond J.R., Cole S., Efstathiou G., Kaiser N., 1991, *ApJ.*, 379, 440
- Cen R., 2003, *ApJ.*, submit. astro-ph/02102473
- Ciardi B., Ferrara A., & White S.D.M., 2003, *MNRAS*, submit. astro-ph/0302451
- Cole S., Hatton, S., Weinberg D.H. and Frenk C., 1998, *MNRAS*, 300, 945
- Cristiani S., D'Odorico V., 2000, *AJ*, 120, 1648
- Croft R.A.C., Weinberg D.H., Katz N., & Hernquist L., 1998, *ApJ.*, 495, 44
- Croft R.A.C. et al., 2002, *ApJ.*, 581, 20
- Davé R., Hernquist L., Katz N., Weinberg D.H., 1999, *ApJ.*, 511, 521,
- Demiański M. & Doroshkevich A., 1999, *MNRAS.*, 306, 779, (DD99).
- Demiański M., Doroshkevich A.G., Müller V., & Turchaninov V.I., 2000, *MNRAS*, 318, 665
- Demiański M. & Doroshkevich A., 2002, astro-ph/0206282, (DD02)
- Demiański M., Doroshkevich A.G., & Turchaninov V.I., 2003, *MNRAS*, 340, 525 (Paper I)
- Djorgovski S.G., Castro S., Stern D., Mahabal A.A., 2001, *ApJ.*, 560, L5
- Doroshkevich, A.G., Tucker, D.L. Fong R., Turchaninov V., & Lin H., 2001, *MNRAS*, 322, 369

- Doroshkevich, A.G., Tucker, D.L. & Allam S., 2002, astro-ph/0206301
- Doroshkevich, A.G., Naselsky I., Naselsky P., Novikov I., 2003, ApJ., 586, 709
- Efstathiou G. et al., 2002, AJ., 122, 8406
- Fan X. et al., 2002, AJ., 123, 1247
- Fan X. et al., 2003, AJ., 125, 1649
- Frenk C.S. 2002, astro-ph/0208219,
- Gnedin N.Y. & Hamilton A.J.S., 2002, MNRAS, 334, 107
- Giallongo E., Cristiani S., Fontana A., & Trevese D., 1993, ApJ., 416, 137
- Hoekstra H., Yee H., & Gladders M., 2002, astro-ph/0204295
- Hu E.M., Tae-Sun K., Cowie L., & Songaila A., 1995, AJ, 110, 1526
- Hui L., 1997, in "Structure and Evolution of the IGM from QSO Absorption Line Systems", Eds. P.Petitjean, S.Charlot, Editions Frontiers, Paris, p. 139
- Hui L., Gnedin N.Y., 1997, MNRAS, 292, 27
- Hui L., Gnedin N.Y., & Zhang Y., 1997, ApJ, 486, 599
- Ivanov P., Naselsky P., & Novikov I., 1994, PhRvD, 50, 7173
- Jacobsen P. et al, 1994, Nature, 370, 35
- Jenkins A. et al., 1998, ApJ., 499, 20.
- Khare P., Srianand R., York D.G., Green R., Welty D., Huang K., & Bechtold J., 1997, MNRAS, 285, 167.
- Kim T.S., Cristiani S., & D'Odorico S., 2002, A&A, 383, 747
- Kim T.S., Carswell R.F., Cristiani S., D'Odorico S. & Giallongo E., 2002, MNRAS, 335, 555
- Kirkman D., & Tytler D., 1997, ApJ., 484, 672.
- Kogut A. et al., 2003, ApJ., submit., astro-ph/0302213
- Komatsu E. et al., 2003, ApJ., submit., astro-ph/0302223
- Kulkarni V.P., Huang K., Green R., 1996, MNRAS, 279, 197
- Lanzetta K.M., Bowen D.V., Tytler D., & Webb J.K., 1995, ApJ., 442, 538.
- Le Brune V., Bergeron J., & Boisse P., 1996, A&A, 306, 691 D.Tytler, in Meylan J., ed., QSO Absorption Lines, p. 289, 1995;
- Loeb A. & Barkana R., 2001, ARA&A, 39, 19
- Lu L., Sargent W.L.W., Womble D.S., Takada-Hidai M., 1996, ApJ., 472, 509
- Matarrese S. & Mohayaee R., 2002, MNRAS, 329, 37
- McDonald P., Miralda-Escude J., Rauch M., Sargent W.L.W., Barlow T.A., Cen R., Ostriker J.P., 2000, ApJ., 543, 1
- McDonald P. & Miralda-Escude J., 2001, ApJ., 549, L11
- McDonald P. et al., 2001, ApJ., 562, 52
- McGill C., 1990, MNRAS, 242, 544
- Meiksin A., Bryan G., & Machacek M., 2001, MNRAS, 327, 296
- Narayanan V. et al., 2000, ApJ., 543, L103
- Naselsky P., & Novikov I., 2002, MNRAS., 334, 137
- Nusser A., Haehnelt M., 2000, MNRAS, 313, 364
- Pando J., Feng L., Jamkhedkar P., Zheng W., Kirkman D., Tytler D., Fang Li-Zhi., 2002, ApJ., 574, 575
- Peacock J.A. & Heavens A.F., 1990, MNRAS, 243, 133
- Peacock J.A. et al., 2001, Nature, 410, 169
- Peiris H.V. et al., 2003, ApJ., submit., astro-ph/0302225
- Pentericci L. et al., 2002, 123, 2151
- Penton S.V., Stocke J.T., & Shull J.M, 2002, ApJ., 565, 720

- Percival W.J et al., 2001, MNRAS, 327, 1297
- Phillips J., Weinberg D.H., Croft R.C., Hernquist L., Katz N., Pettini M., 2001, ApJ., 560, 15
- Polarski D., & Starobinsky A.A., 1995, Phys.Lett., B356, 196
- Press W.H., & Schechter P., 1974, ApJ, 187, 425
- Rodriguez-Pascual P.M., de la Fuente A., 1995, ApJ., 448, 575.
- Schaye J.et al., 2000, MNRAS, 318, 817
- Scott J., Bechtold J., Dobrzycki A. & Kulkarni V.P., 2000, ApJSupl, 130, 67
- Seljak U., McDonald P., & Makarov A., 2003, MNRAS, submit. astro-ph/0302571
- Shandarin S., Zel'dovich Ya.B., 1989, Rev.Mod.Phys., 61, 185
- Schmalzing J., Gottlöber S., Klypin A., Kravtsov A., 1999, MNRAS, 309, 1007
- Sommer-Larsen J. et al., 2003, in preparation
- Spergel D.N. et al., 2003, ApJ., submit., astro-ph/0302209
- Tegmark M. Hamilton A.J.S. & Xu Y., 2002, MNRAS, 335,432
- Tegmark M. and Zaldarriaga M., 2002, Phys.Rev.D, in press, Astro-ph/0207047
- Theuns T., Leonard A., Schaye J., Efstathiou G., 1999, MNRAS, 303, L58
- Theuns T., Schaye J., Zaroubi S., Kim T.-S., Tzanavaris P., & Carswell R., 2002a, ApJ, 567, L103
- Theuns T., Zaroubi S., Kim T.-S., Tzanavaris P., & Carswell R., 2002b, MNRAS, 332, 367
- Turok N., ApJ., 473, L5
- Tytler D., 1995, in Meylan J., ed., QSO Absorption Lines, p. 289.
- Verde L. et al., 2002, MNRAS, 335, 432
- Wang X., Tegmark M., Jain B. and Zaldarriaga M., 2002, Astro-ph/0212417
- Weinberg D.H. et al., 1998, in "Evolution of Large Scale Structure: From Recombination to Garching", eds. A.J. Banday, R.K. Sheth, L.N. Da Costa, p. 346
- White M. and Croft R.A.C., 2003, astro-ph/0001247
- Zaldarriaga M., Scoccimorro R., Hui L., 2002, astro-ph/0111230
- Zaldarriaga M., Hui L. & Tegmark M., 2001, ApJ., 557, 519
- Zel'dovich Ya.B., 1970, Astrophysica, 5, 20
- Zeng W., Davidsen A.F., & Kriss G.A., 1998, AJ, 115, 391
- Zhang Yu., Meiksin A., Anninos P., Norman M.L., 1998, ApJ., 495, 63

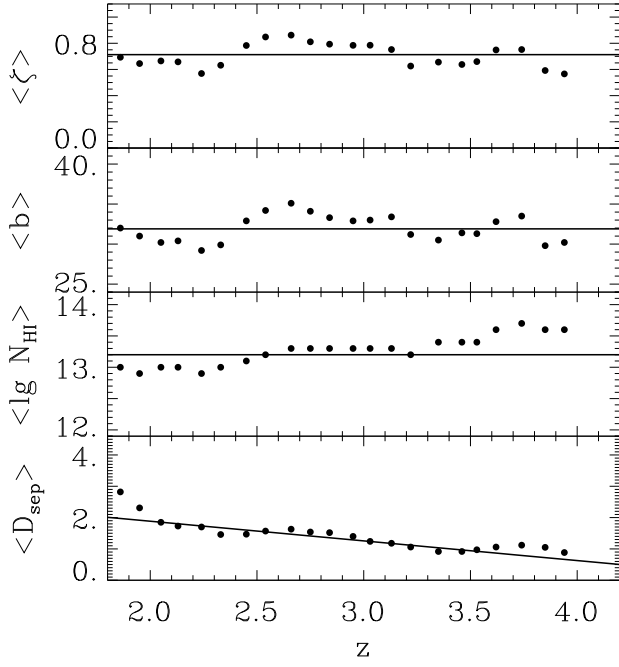


Fig. 1.— The mean DM column density of absorbers, $\langle \zeta \rangle$, the mean Doppler-parameter, $\langle b \rangle$ (in km/s), the mean neutral hydrogen column density, $\langle \log N_{HI} \rangle$ and the mean absorber separations, $\langle D_{sep} \rangle h^{-1} \text{Mpc}$, are plotted vs. redshift z . Fits (31) are plotted by solid lines.

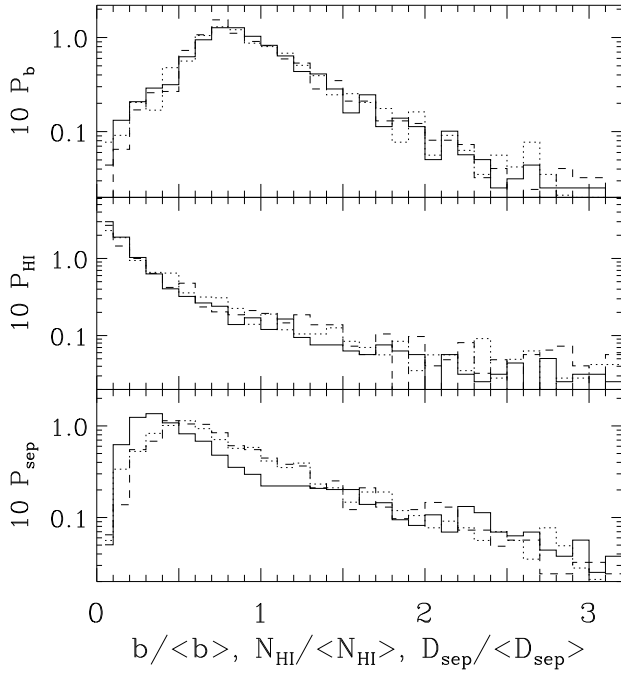


Fig. 2.— PDFs for the Doppler parameter, P_b , the hydrogen column density, P_{HI} , and absorbers separation, P_{sep} , for redshift 1.7 – 2.5 (solid lines), 2.5 – 3 (dot lines) and 3 – 4.5 (dashed lines).

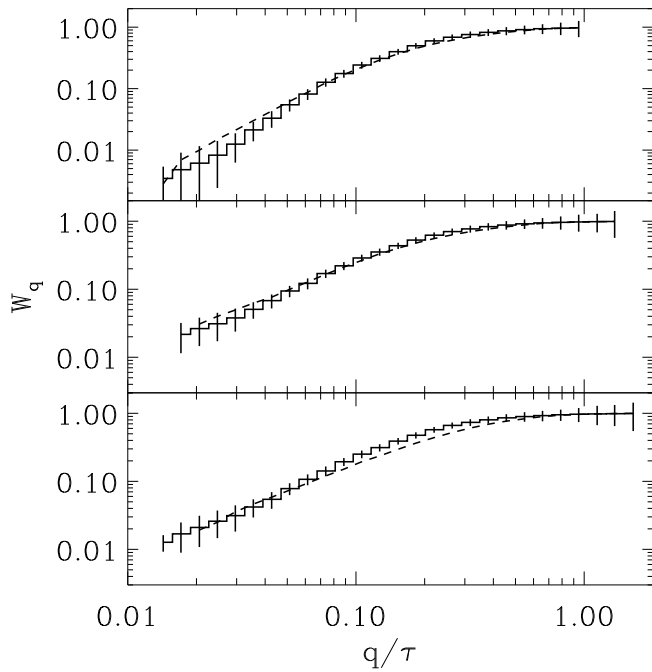


Fig. 3.— Cumulative distribution functions, W_q , are plotted vs. q/τ for Model 1 (top panel), Model 2 (middle panel) and Model 3 (bottom panel). In the same panels, the best fits (38) are plotted by solid lines.

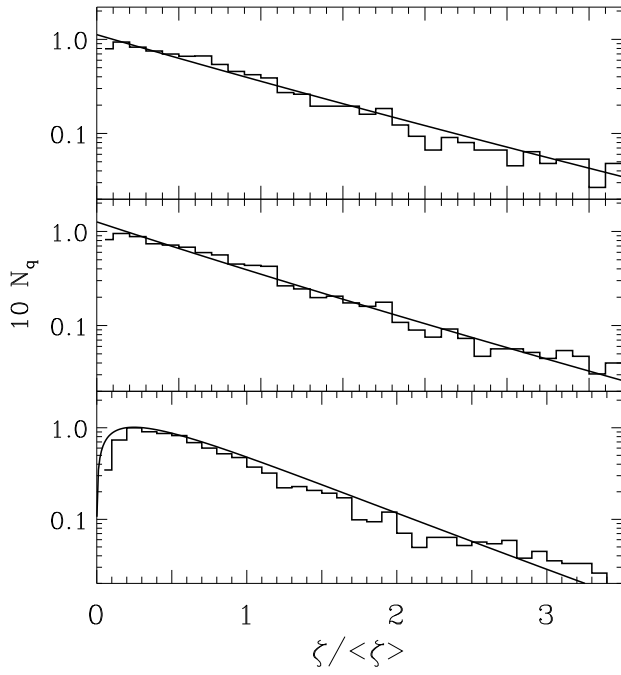


Fig. 4.— PDFs, N_q , for the Model 1 (top panel), the Model 2 (middle panel) and the Model 3 (bottom panel) are plotted vs. $\xi / \langle \xi \rangle$. Solid lines shows fits (14) and (15) for ξ_v given by (38).

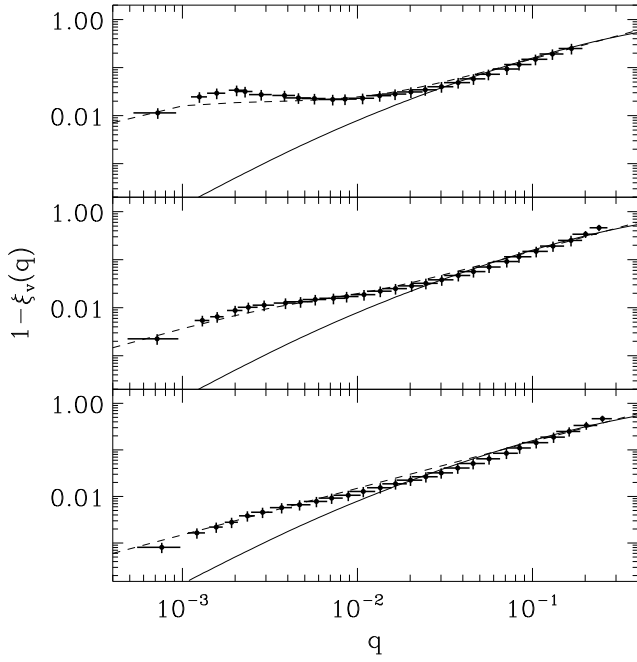


Fig. 5.— Correlation function of the initial velocity field, $\xi_v(q)$, for the Model 1 (top panel), Model 2 (middle panel) and Model 3 (bottom panel). Dashed and solid lines show fits (38) and the function ξ_{CDM} (10).

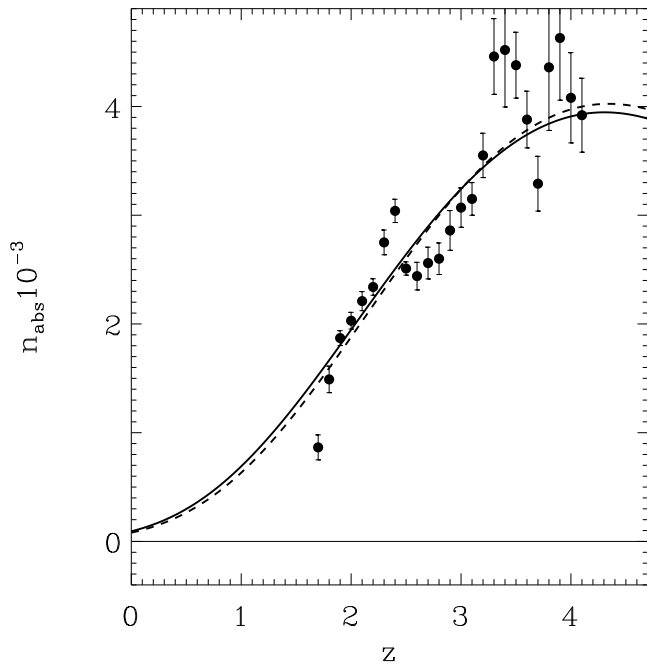


Fig. 6.— Redshift distribution of absorbers, $\langle n_{abs}(z) \rangle$, for 4500 observed absorbers. Fits (16) for Model 1 and Model 3 are plotted by solid and dashed lines.

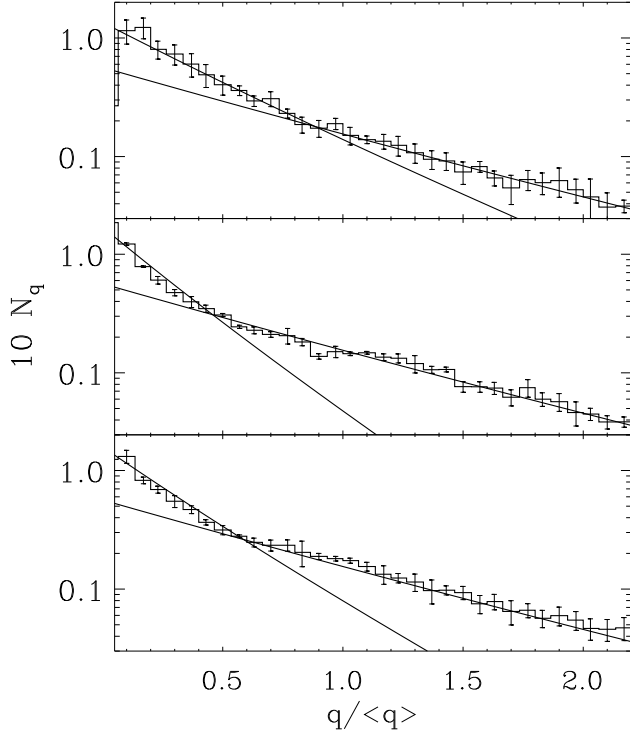


Fig. 7.— The PDFs of dimensionless surface density of walls, N_q , for 3 sets of walls selected from two high resolution DM simulations with small threshold richness. Fits (14) are plotted by solid lines.

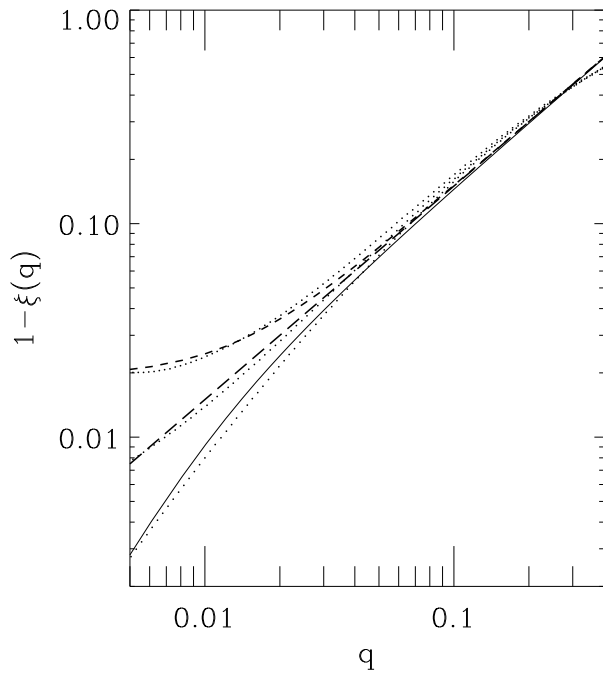


Fig. 8.— Correlation functions for the initial velocity field (10) (solid line) and (38) for the Model 1 and Model 3 (dashed and long dashed lines) together with the same functions for spectra (47) and (48) (dotted lines).

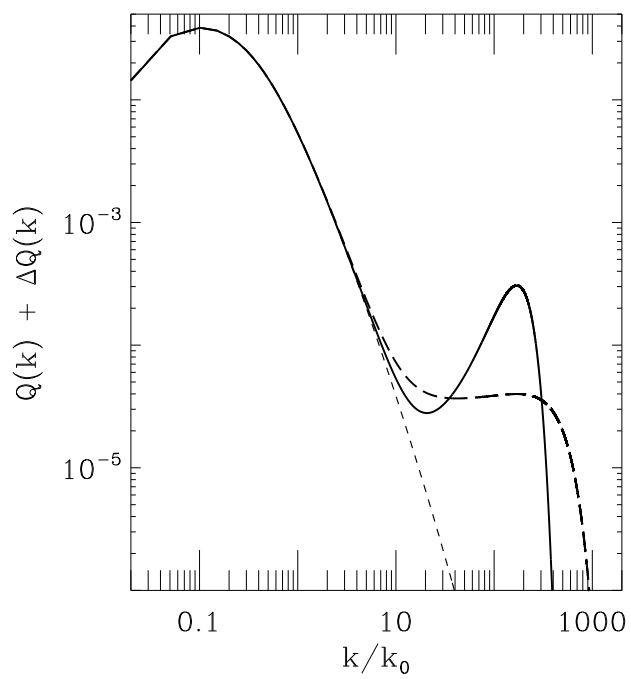


Fig. 9.— Normalized total initial power spectrum for two sets of parameters (48) (solid and long dashed lines) and CDM-like one (47) (dashed line).

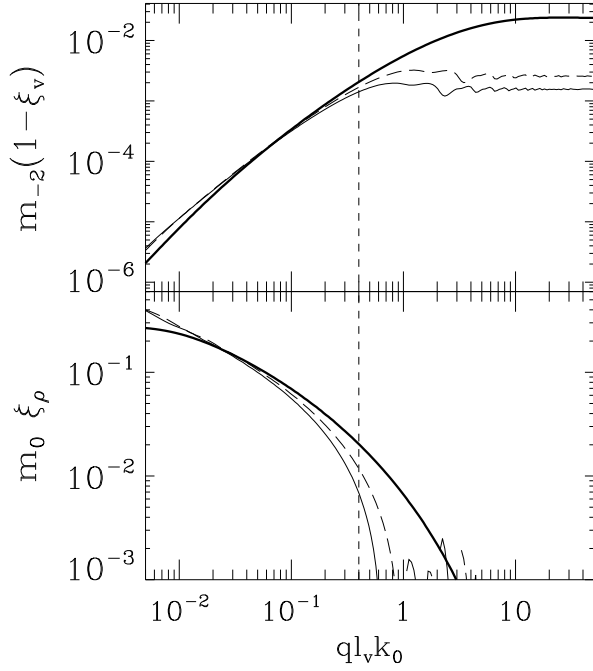


Fig. 10.— Normalized correlation functions of initial velocity and density fields, ξ_v & ξ_ρ , vs. the dimensionless point separation, $ql_v k_0$, for the CDM-like power spectrum (thick solid line) and for truncated spectra used in simulations with 256^3 cells and the box sizes $k_0 L_{box} = 2.1$ (thin solid line) and 3.14 (long dashed line).

Table 1: QSO spectra used in our analysis

	z_{em}	z_{min}	z_{max}	No of HI lines
0000 – 260 ¹	4.11	3.4	4.1	431
0055 – 259 ²	3.66	3.0	3.6	534
0014 + 813 ³	3.41	2.7	3.2	262
0956 + 122 ³	3.30	2.6	3.1	256
0302 – 003 ^{3,2}	3.29	2.6	3.1	356
0636 + 680 ³	3.17	2.5	3.0	313
1759 + 754 ⁴	3.05	2.4	3.0	307
1946 + 766 ⁵	3.02	2.4	3.0	461
1347 – 246 ²	2.63	2.1	2.6	361
1122 – 441 ²	2.42	1.9	2.4	353
2217 – 282 ²	2.41	1.9	2.3	262
2233 – 606 ⁶	2.24	1.5	2.2	293
1101 – 264 ²	2.15	1.6	2.1	277
0515 – 441 ²	1.72	1.5	1.7	76

1. Lu et al. (1996), 2. unpublished, courtesy of Dr. Kim 3. Hu et al., (1995), 4. Djorgovski et al. (2001) 5. Kirkman & Tytler (1997), 6. Cristiani & D’Odorico (2000).